THE JOURNAL OF BIOLOGICAL CHEMISTRY VOL. 288, NO. 12, pp. 8544–8559, March 22, 2013

Cyr61, a Matricellular Protein, Is Needed for Dendritic Arborization of Hippocampal Neurons*[S]

Received for publication, August 17, 2012, and in revised form, January 23, 2013 Published, JBC Papers in Press, January 28, 2013, DOI 10.1074/jbc.M112.411629

Anna R. Malik[‡], Malgorzata Urbanska[‡], Agata Gozdz[‡], Lukasz J. Swiech[‡], Andrzej Nagalski[§], Malgorzata Perycz[‡], Magdalena Blazejczyk[‡], and Jacek Jaworski[‡1]

From the [‡]Laboratory of Molecular and Cellular Neurobiology and the [§]Laboratory of Neurodegeneration, International Institute of Molecular and Cell Biology, 4 Ks. Trojdena St., 02-109 Warsaw, Poland

Background: Cyr61 is an angiogenic protein with unknown neuronal function expressed in the developing nervous system.
Results: Knockdown and overexpression of Cyr61 affect dendritic arbor morphology.
Conclusion: Cyr61 is necessary to control dendritic morphology.
Significance: The function of Cyr61 in neurons has been identified for the first time.

The shape of the dendritic arbor is one of the criteria of neuron classification and reflects functional specialization of particular classes of neurons. The development of a proper dendritic branching pattern strongly relies on interactions between the extracellular environment and intracellular processes responsible for dendrite growth and stability. We previously showed that mammalian target of rapamycin (mTOR) kinase is crucial for this process. In this work, we performed a screen for modifiers of dendritic growth in hippocampal neurons, the expression of which is potentially regulated by mTOR. As a result, we identified Cyr61, an angiogenic factor with unknown neuronal function, as a novel regulator of dendritic growth, which controls dendritic growth in a β1-integrin-dependent manner.

The electrical properties of neurons are regulated by the composition and density of synapses and pattern of dendritic branching (1, 2). In mammals, the development of a proper dendritic branching pattern strongly relies on extracellular cues, such as neurotransmitters, trophic factors, the extracellular matrix, and cell adhesion molecules and the subsequent adjustment of the dynamics of intracellular processes that underlie dendrite growth and stability (3, 4). The Ras-phosphoinositide 3-kinase (PI3K) and Ras-extracellular signal-regulated kinase (ERK) signaling pathways were previously shown to contribute to brain-derived neurotrophic factor (BDNF)[2]-driven dendritic arborization, most likely via activation of mTOR and its downstream effector p70S6K1 (S6K1) (5). The S6K1-dependent translation of cytoskeleton-regulating proteins was shown to be sufficient to drive axonal growth (6). It remains unknown, however, whether a similar situation occurs during dendrite growth or whether other mTOR-dependent cellular processes are also required.

For many years, mTOR and its homologs (TORs) were considered solely regulators of protein synthesis. Several reports, however, indicated a major role of TOR in the regulation of transcription. Yeast TOR1 is known to control transcription driven by all three RNA polymerases (7). In *Drosophila melanogaster*, large scale profiling provided evidence that dTOR controls the expression of dozens of genes (8). Research in mammals identified transcription factors, the activity or expression of which are regulated by mTOR (*e.g.* YY-1 (yin-yang 1), sterol regulatory element-binding protein, Maf1, and HIF1α (hypoxia-inducible factor-1α)) (9–12). YY-1, sterol regulatory element-binding protein, and HIF1α were also shown to play important roles in physiological or pathological neuronal transmission (13–15). Moreover, the transcriptional profiling of cells with increased mTOR signaling, like neuroepithelial cells that lack TSC2 or subependymal giant-cell astrocytomas derived from tuberous sclerosis patients revealed differences in the expression of several genes that are important for neuronal development (16, 17).

Matricellular proteins are secreted proteins that are closely associated with the extracellular matrix. Rather than being structural components of the extracellular matrix, however, such proteins contribute to cell signaling by acting as modulators of cell surface receptors. For example, Cyr61 (cysteine-rich 61; CCN1), a member of the CCN (Cyr61/CTGF/NOV) family of matricellular proteins, is a ligand of different integrins (18–20). Through these interactions it regulates cell adhesion, migration, proliferation, survival, apoptosis, differentiation, gene expression, and senescence, depending on the cell type and particular integrin involved (21, 22). Although Cyr61 is mostly known for its roles in various non-neuronal cells (21), it is also expressed in the developing nervous system and neuron-like cells (23, 24). Nonetheless, knowledge about the function of this protein in neurons is very limited. Thus far, the only functional data have come from the work of Kim *et al.* (24), who showed that knockdown of Cyr61 decreased the etoposide-in-

* This work was supported by FP-7 Health-Prot Grant 229697, ERA-NET-Neuron/03/2010 (co-financed by the National Center for Research and Development) and National Science Center Grant OPUS 2011/03/B/NZ3/01970 (JJ). Also co-financed by European Union funds from European Social Fund (M.U.).

[S] This article contains supplemental Tables 1–3.

[1] To whom correspondence should be addressed. Tel.: 48-22-597-07-55; Fax: 48-22-597-07-15; E-mail: jaworski@iimcb.gov.pl.

[2] The abbreviations used are: BDNF, brain-derived neurotrophic factor; mTOR, mammalian target of rapamycin; DIV, day *in vitro*; TNDT, total number of dendritic tips; TDL, total dendritic length; S6K1, p70 S6 kinase 1; mRFP, monomeric red fluorescent protein; E*n*, embryonic day *n*; P*n*, postnatal day *n*; RT-qPCR, reverse transcription quantitative polymerase chain reaction; ANOVA, analysis of variance; ActD, actinomycin D.

duced death of immortalized hippocampal progenitor H19-7 cells, suggesting a role of Cyr61 in neuronal cell death. In addition to this observation, the function of Cyr61 in neurons, especially during their development, is unknown, but several factors that induce *cyr61* expression and transcription factors that regulate *cyr61* transcription are known for their contribution to neuronal development and plasticity (see below).

cyr61 is an immediate early gene, the transcription of which is induced by numerous stimuli, including trophic factors (*e.g.* epidermal growth factor (EGF) and fibroblast growth factor (FGF)) (24, 25), Wnt (26), hypoxia (27), and mechanical stretch (28). The neuronal expression of *cyr61* has not been studied thoroughly, but the activity of the *cyr61* promoter was detected in the developing central nervous system of reporter mouse embryos that carried the β-galactosidase (β-gal) coding sequence under the *cyr61* promoter (23). It has also been shown that in H19-7 cells, *cyr61* expression can be induced by neurotransmitter glutamate, *N*-methyl-D-aspartate (NMDA), an agonist of NMDA-type glutamate receptors and proapoptotic drug etoposide (24). Etoposide induced *cyr61* transcription, activating c-Jun N-terminal kinase (JNK) and serum response factor (SRF). Besides these observations, the regulation of *cyr61* transcription in neurons under more physiological conditions remains rather unexplored.

In this work, we first showed that S6K1, the best known mTOR effector, is not sufficient to induce dendritic arbor development. Consequently, we performed short hairpin RNA (shRNA) screening to identify genes that are involved in the regulation of dendritic arbor shape, the expression of which is potentially regulated by mTOR. In this screen, we identified *cyr61*, which is expressed in developing neurons in a trophic factor-, Ras-, ERK-, and PI3K-dependent manner. Knockdown of Cyr61 prevented dendritic growth under basal conditions and dendritic growth induced by insulin, Ras, and PI3K. We also showed that overexpressed Cyr61 induces dendritic growth in a β1-integrin-dependent manner.

EXPERIMENTAL PROCEDURES

Antibodies and Drugs—The mouse anti-Tau (PHF-1) antibody was described previously and kindly provided by Dr. Davies (29). The following antibodies were obtained from commercial sources: rat anti-HA (Roche Applied Science), mouse anti-α-tubulin, mouse anti-MAP2 (Sigma), rabbit anti-GFP (Medical and Biological Laboratories, Woburn, MA), rabbit anti-phospho-S6 (Ser-235/236), rabbit anti-MAP2 (Cell Signaling Technology, Danvers, MA), mouse anti-β-galactosidase (Promega, Madison, WI), mouse anti-GAD67 (Millipore, Billerica, MA), mouse anti-Tau (Tau-1) (Cedarlane, Burlington, Canada), hamster anti-CD29 (β1-integrin chain), and isotype IgM (BD Biosciences). Anti-mouse or anti-rabbit secondary antibodies conjugated to Alexa Fluor 488, Alexa Fluor 568, and horseradish peroxidase (HRP) were obtained from Invitrogen and Jackson ImmunoResearch (West Grove, PA), respectively. Wortmannin and rapamycin were obtained from Calbiochem. Insulin, BDNF, bicuculline, and actinomycin D were purchased from Sigma. UO126 was purchased from Promega.

DNA Constructs—The following mammalian expression plasmids have been described previously: pSuper vector (30), β-actin-GFP (encoding EGFP under control of the β-actin promoter), p110CAAX, GW1-HA-RasV12, GW1-HA-RasV12S35, GW1-HA-RasV12S40, pSuper-mTOR7513 (5), β-actin-mRFP (encoding mRFP under the control of the β-actin promoter) (31), EFα-β-gal (32), and pRK5-Myc-S6K1T389E (33). The β-actin-TdTomato, encoding TdTomato under control of the β-actin promoter, was obtained by subcloning TdTomato coding sequence (34) to modified β-actin-16pl (35). The sequences that encode the shRNAs used in the screen were cloned into pSuper and are listed in supplemental Table 1. Scrambled shRNAs were designed based on the original Cyr61 siRNA sequences using the online siRNA Wizard version 3.1 tool and cloned into pSuper vector. The following sequences were used: 5′-GATGTACGTACATCTACTC-3′ (Cyr61scr#1); 5′-GGGTGAGATCATGAGAGAA-3′ (Cyr61scr#2); 5′-AGCTCTTAGGCTTGTATA-3′ (Cyr61scr#3). The coding sequence of *cyr61* was obtained by PCR using RAT2 cell cDNA, and the product was cloned into pJET1.2 (Fermentas, Burlington, Canada) according to the manufacturer's instructions. The pJET-Cyr61 plasmid was next used for the preparation of a template for the cRNA probe with the use of the following primers that contained promoter sequences for T3 or T7 RNA polymerases on their ends: cyr61T7 (5′-TAATACGACTCACTATAGGGATGAGCTCCAGCACCATCAAGACGCTCGCTGTCGC-3′) and cyr61T3 (5′-AATTAACCCTCACTAAAGGGGTCCCTGAACTTGTGGATATCGTTGAACAGACTG-3′). pJet-Cyr61 was also used as a PCR template to obtain Cyr61 coding sequence for preparation of β-actin-Cyr61-GFP. The obtained PCR product was cloned to EcoRI and SalI sites of β-actin-GFP with modified multicloning site.

Cell Cultures, Transfection, and Drug and Antibody Treatments—The animals used to obtain neurons for tissue cultures and RNA from brain extracts were sacrificed according to the protocols approved by the First Ethical Committee (Warsaw, Poland). Primary hippocampal and cortical cultures were prepared from embryonic day 19 (E19) rat brains and transfected using the Lipofectamine2000 (Invitrogen) or Amaxa nucleofection procedure as described recently (36, 37). For the shRNA library screening, the neurons were transfected with pools of plasmids that encode shRNAs that target a given gene and GFP-encoding vector in the following proportions: 2:2:2:3 (shRNA#1/#2/#3/GFP) or 3:3:3 (shRNA#1/#2/GFP, in the case that only two shRNAs were used to silence a given mRNA). For insulin-induced dendritic growth, immediately after transfection, the neurons were transferred to a regular culture medium that contained a reduced concentration of B27 (0.2% instead of 2%; Invitrogen). Insulin (400 nM) was added for the first time 4 h after transfection and then every 24 h until cell fixation. To inhibit the β1-integrin receptor, the neurons were treated with anti-CD29 antibody or isotype control twice (2 and 4 days after transfection) at a concentration of 20 μg/ml. To induce *cyr61* expression, hippocampal neurons were treated with BDNF (100 ng/ml), insulin (400 nM), and bicuculline (50 μM) for 1 h. Neurons on day *in vitro* 8 (DIV8) prior to stimulation were kept overnight in a culture medium with 0.2% B27. DIV21 neurons were treated with these drugs after a 4-h incubation in a culture medium without B27. Actinomycin D (1 μg/ml), UO126 (20

μM), wortmannin (1 μM), or DMSO (control) was added to the medium 45 min prior to insulin or BDNF.

RAT2 cells were cultured as described previously (36). To obtain high transfection efficiency, 2.2×10^6 RAT2 cells were suspended in 100 μl of phosphate-buffered saline (PBS) and nucleofected with 6 μg of DNA using an Amaxa Nucleofector II Device (Lonza, Koln, Germany; X-005 program).

shRNA Library Screen—Hippocampal neurons were transfected on DIV8 with pools of shRNAs that targeted the chosen mRNA as described above. Four days after transfection, the neurons were fixed with 4% paraformaldehyde and 4% sucrose in PBS and immunostained for GFP. Each culture plate contained control variants transfected with pSuper or plasmid that encoded mTOR shRNA. To avoid variability caused by differences between cultures, the total number of dendritic tips (TNDT) was quantified as a percentage of the mean value obtained for neurons transfected with empty pSuper from the same experimental plate. Two independent screening experiments were performed, and the mean value was calculated from both of them for each shRNA pool.

Immunocytochemistry of Hippocampal Neurons—For the immunofluorescent staining of P-S6, the neurons were fixed with 4% paraformaldehyde that contained 4% sucrose in PBS for 10 min at room temperature. Afterward, staining was performed according to the manufacturer's protocol (Cell Signaling Technology). The immunostaining of MAP2, Tau, GAD67 and transfected proteins was performed as described previously (36).

RNA Isolation and Reverse Transcription Quantitative Polymerase Chain Reaction (RT-qPCR)—RNA from cultured neurons and rat hippocampi was isolated with the RNeasy Protect minikit (Qiagen). cDNA was prepared with High Capacity RNA-to-cDNA Master Mix (Applied Biosystems) according to the manufacturer's protocol. qPCR was performed using a 7900HT real-time PCR system and TaqMan gene expression assays (Applied Biosystems) with the following TaqMan rat probes: GAPDH (Rn99999916_s1) and Cyr61 (Rn01523136_g1). The results were analyzed by the comparative *Ct* method for relative quantification. SDS version 2.4 and RQ Manager version 1.2.1 programs were used for data acquisition and preliminary analysis.

In Situ Fluorescent Hybridization—For *in situ* fluorescent hybridization, the cells were fixed in 4% paraformaldehyde for 10 min at room temperature and incubated with 1% H_2O_2 to minimize background. After washing with PBS that contained diethylpyrocarbonate, the cells were first incubated for 1 h at room temperature with prehybridization buffer (50% (v/v) formamide, 4 μg/ml *Escherichia coli* tRNA, 2% (v/v) Denhardt's solution (Sigma-Aldrich), 1% (v/v) salmon sperm DNA (Sigma-Aldrich), and 2 mM ribonucleoside vanadyl complexes (Sigma-Aldrich)) and then with hybridization buffer (2× SSC, 50% (v/v) formamide, 10% dextran sulfate, 4 μg/ml *E. coli* tRNA, 2% (v/v) Denhardt's solution, 1% (v/v) salmon sperm DNA, and 2% (v/v) ribonucleoside vanadyl complexes) that contained 1.5 ng/μl of heat-denaturated digoxigenin-labeled single-stranded sense or antisense RNA probes for 10 h at 56 °C. After the hybridization step, the cells were rinsed in 2× SSC, washed once in 2× SSC for 1 h at 56 °C, washed twice in 0.2× SSC for 30 min at 56 °C, and washed four times in 0.2× SSC for 30 min at room temperature. The immunofluorescent detection of digoxigenin-labeled probes was then performed using HRP-conjugated anti-digoxigenin antibody (Roche Applied Science) and the Tyramide Signal Amplification (TSA) Plus Cyanine 5 System (PerkinElmer Life Sciences). For fluorescent *in situ* hybridization (FISH), we used cRNA probes synthesized and labeled using the digoxigenin RNA labeling Kit (SP6/T7) (Roche Applied Science) and T3 polymerase (Roche Applied Science). The full coding sequence of *cyr61* was obtained by PCR using pJet-Cyr61 and used as a template. The primers used for the PCR contained promoter sequences for T3 or T7 RNA polymerases on their ends.

Image Analysis and Quantification—Confocal neuron images were obtained with a Zeiss LSM5 Pascal or LSM710NLO microscope at 1024 × 1024-pixel resolution for morphological analysis. The ×10, ×20, and ×40 objectives were used. Each image consisted of a series of *z*-stack images. The resultant stack was flattened into a single image using maximum projection. The confocal settings were constant for all of the scans when fluorescence intensity was compared. Morphometric analysis and quantification were performed with MetaMorph image analysis software (Universal Imaging Corp., Downingtown, PA) for the manual counting of total number of dendritic tips and ImageJ software with the NeuronJ plug-in (38) and Sholl plug-in (available on the University of California, San Diego, The Ghosh Lab Web site) for measurements of total dendrite length and Sholl analysis, respectively. Briefly, we used the tracking function in NeuronJ to manually draw a mask of all dendrites of the transfected neuron on a confocal image and measured their length. If more than one transfected cell was present at the particular image, the mask was created only for a single cell. The mask was saved as a separate image and used in the automated Sholl analysis to avoid background of axons and other cells whose fragments could be present in the original pictures. The original script of the Sholl plug-in was modified for more accurate performance with masks instead of raw images. Images of axonal arbors were obtained with a Nikon Eclipse 80i microscope equipped with a ×10 objective, monochromatic Evolution VF charge-coupled device camera (Media Cybernetics, Silver Spring, MD), and ImageProPlus software (Media Cybernetics). For the analysis of the total length of the axons, ImageJ software with the NeuronJ plug-in was used. Dendrites and axons were primarily distinguished by morphological criteria (*i.e.* "short" neurites with decreasing diameter, splitting with narrow splitting angles (usually smaller than 90°) were treated as dendrites, whereas "long" neurites with relatively constant diameter splitting with variable splitting angles (often equal to or larger than 90°) were scored as axons). The additional criterion helpful for discrimination between dendrites and axons was the presence of dendritic filopodia and dendritic spines. The accuracy of morphology-based classification was additionally confirmed in selected cases (Cyr61 knockdown, Cyr61 overexpression, S6K1T389E overexpression) with immunofluorescent staining for MAP2 (marker of dendrites), Tau-1 (marker of axons of DIV0–3 neurons), and PHF-1 (marker of axons of >DIV5 neurons), as suggested previously (39). For the measurements of mean fluores-

cence intensity, MetaMorph image analysis software was used. Immunofluorescence intensities were measured as described previously (33). In the case of FISH analysis, the mean fluorescence signal from transfected cells was standardized to the signal from non-transfected cells from the same field of view.

Statistical Analysis—The data were obtained from at least three batches of cells, with the exception of the screening experiment that was performed on two batches of neurons. The exact numbers of neurons and examined for the morphology analyses are provided in the respective figure legends and in supplemental Table 2. The statistical analyses were performed using Prism (GraphPad, San Diego, CA). The Kruskal-Wallis test followed by Dunn's post hoc test, a two-way ANOVA test followed by Bonferroni's post hoc test, a one-way ANOVA test followed by Tukey's multiple comparison test, the Mann-Whitney test, a paired *t* test, or a one-sample *t* test was used, depending on the type of data analyzed.

RESULTS

Overexpression of S6K1 Is Not Sufficient to Induce Dendritic Growth—We previously showed that S6K1 is needed for the development of the dendritic arbor of hippocampal neurons in dissociated culture and hippocampal slices (5). To investigate whether S6K1 activation is sufficient to induce dendritic growth, DIV8 hippocampal neurons were transfected with a plasmid that encoded a hyperactive mutant of S6K1 (S6K1T389E). Transfection with plasmids that encoded β-gal and constitutively active PI3K (p110CAAX) served as negative and positive controls, respectively. In all of the variants, the plasmid that encoded GFP was cotransfected to visualize the morphology of transfected cells (Fig. 1*A*). The cells were fixed on DIV14. The analysis of the TNDT revealed no differences between neurons that overexpressed β-gal and S6K1T389E (Fig. 1*B*). p110-CAAX, in contrast, caused a 60% increase in dendritic tips (Fig. 1, *A* and *B*) as described previously (5, 40), demonstrating the capability of the tested neurons to express dendritic arbor expansion. A TNDT is a very simplified measure that potentially could miss some subtle changes in dendritic arbor morphology. Therefore, we performed analysis of additional parameters that describe dendritic arbor morphology (*i.e.* measurement of total dendritic length (TDL) and Sholl analysis). Sholl analysis (41), which measures the number of dendrites that cross circles at various radial distances from the cell soma, describes changes in dendritic arbor complexity and the area of a dendritic field. Downward and leftward shifts of the Sholl plot correspond to the decreased complexity and shrinkage of dendritic arbors. Upward and rightward shifts, in contrast, reflect the increased complexity and expansion of the dendritic field. As shown in Fig. 1, *C* and *D*, also such additional analyses did not reveal an effect of S6K1T389E overexpression on proper dendritic arbor morphology. On the other hand, S6K1T389E was able to induce the phosphorylation of its downstream effector, ribosomal protein S6, on serines 235 and 236 (Fig. 1, *E* and *F*). S6K1T389E was also sufficient to induce axonal growth (Fig. 1, *G* and *H*) when transfected in DIV0 neurons for 3 days, as described previously for other hyperactive S6K1 mutants (6). These experiments demonstrated that S6K1T389E was biologically active in our preparations. Thus,

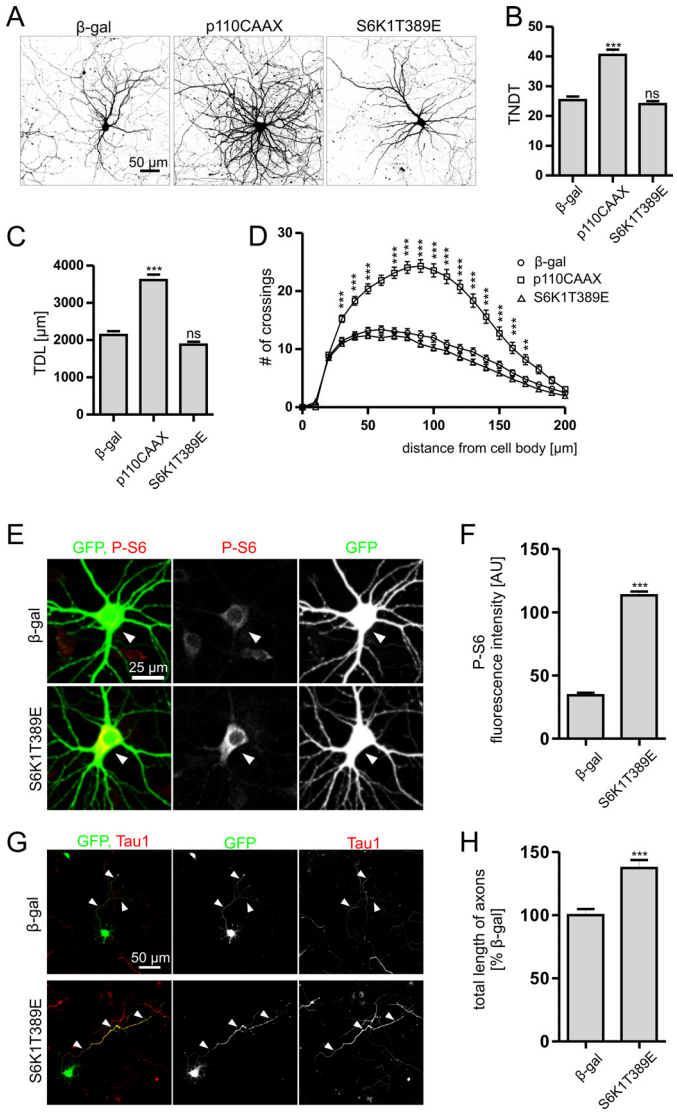

FIGURE 1. **Expression of constitutively active S6K1 is not sufficient to induce dendritogenesis.** *A*, representative images of cultured *in vitro* hippocampal neurons transfected on DIV8 for 7 days with plasmids that encode β-gal, p110CAAX or S6K1T389E. The cells were cotransfected with a GFP-coding vector for the visualization of neuronal morphology. *Scale bar*, 50 μm. Shown are TNDT (*B*), TDL (*C*), and Sholl analysis (*D*) of cells transfected as described in *A* (β-gal, $n = 45$; p110CAAX, $n = 41$; S6K1T389E, $n = 45$). Cell images were obtained from three independent culture batches. *Error bars*, S.E. ***, $p < 0.001$, compared with β-gal (Kruskal-Wallis test followed by Dunn's post hoc test for *B* and *C*; two-way ANOVA test followed by Bonferroni's post hoc test for *D*); *ns*, not significant. *E*, representative images of cultured *in vitro* hippocampal neurons transfected on DIV8 for 3 days with vectors that encode either β-gal or S6K1T389E and immunostained for P-S6 (Ser-235/236). GFP-encoding plasmid was cotransfected for the visualization of transfected cells. *Scale bar*, 25 μm. *F*, quantification of P-S6 immunofluorescence (β-gal, $n = 60$; S6K1T389E, $n = 57$). Cell images were obtained from three independent culture batches. *Error bars*, S.E. ***, $p < 0.001$ (Mann-Whitney test). *AU*, arbitrary units. *G*, representative images of hippocampal neurons cultured *in vitro* and transfected on DIV0 for 3 days with plasmids that encode either β-gal or S6K1T389E together with one that encodes GFP (*green*) and immunofluorescently labeled with anti-Tau1 antibody to highlight axons (*red*). The *arrowheads* point to Tau1-positive neurites. *Scale bar*, 50 μm. *H*, mean length of axons, classified based on morphological criteria, expressed as a percentage of the mean value for β-gal-transfected control neurons (β-gal, $n = 67$; S6K1T389E, $n = 69$). Cell images were obtained from three independent culture batches (different from *G*). *Error bars*, S.E. ***, $p < 0.001$ (Mann-Whitney test).

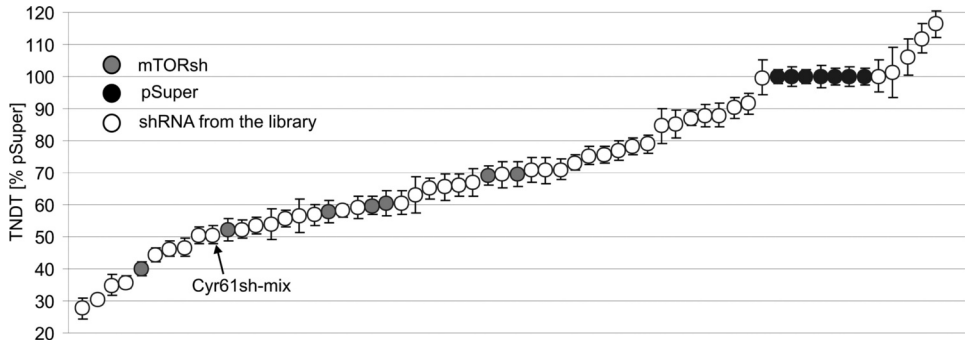

FIGURE 2. **shRNA screening results indicate that Cyr61 is a possible mTOR effector involved in dendritogenesis.** Shown are the results of screening for possible mTOR effectors involved in dendritogenesis. Hippocampal neurons cultured *in vitro* were transfected on DIV8 for 4 days with pSuper vectors that encode pools of two or three shRNAs that target mRNAs possibly regulated by mTOR at the level of transcription. A GFP-encoding plasmid was cotransfected for the visualization of transfected neurons. As controls, empty pSuper or pSuper-mTOR7513 (encoding mTORsh) was transfected to neurons on each culture plate. The plot represents the mean TNDT ± S.E. (*error bars*) obtained in two independent experiments, expressed as a percentage of a corresponding pSuper-transfected negative control from the same culture plate.

we conclude that S6K1 activity is not sufficient to drive dendritic growth, unlike in the case of axonal development.

Several Genes, the Expression of Which Potentially Depends on mTOR, Are Needed for Proper Dendritic Arbor Morphology—Because S6K1 was not sufficient to drive dendritic growth, we searched for new potential mTOR effectors needed for this process. Recent phosphoproteomic studies identified several regulators of transcription and mRNA processing among mTOR substrates (43, 44). Therefore, we decided to test whether the genes that encode mRNAs whose levels were previously shown to depend on mTOR activity (8, 16, 17) are involved in dendritic arbor development. To achieve this, we designed a minilibrary of shRNAs that target 46 such mRNAs (supplemental Table 1) using algorithms that proved to be accurate in over 66% of the cases in our previous studies (*i.e.* two of three designed shRNAs were effective) (5, 36, 37). These shRNAs were cloned into pSuper vector. Hippocampal neuronal cells were then transfected on DIV8 with pools of shRNAs that targeted each selected mRNA for 4 days. The plasmid that encoded GFP was cotransfected to help identify transfected cells and visualize their morphology. Two control variants were included on each experimental plate. As a negative control, we used cells transfected with empty pSuper. As a positive control, we transfected cells with pSuper-mTOR7513 (5). To assess changes in dendritic arbors, we quantified TNDT. As expected from our previous studies (5), transfection with pSuper-mTOR7513 caused a drop in TNDT compared with pSuper-transfected neurons (Fig. 2; also see supplemental Table 2). Several tested pools of shRNAs (16 of 46) caused a significant decrease in TNDT ($p < 0.01$) in each of the two experiments (for details, see supplemental Table 2). For these pools, the effects ranged from a 23% to a 72% decrease in TNDT compared with the negative control (supplemental Table 2). Among the positive shRNA pools, we decided to focus on one that targeted mRNA that encoded matricellular protein Cyr61 for further functional evaluation.

Cyr61 Expression in Neurons—The expression and function of Cyr61 have not been previously studied in developing neurons. Therefore, before going into more detail of the involvement of Cyr61 in dendritic arborization, we decided to better characterize the *cyr61* expression profile in neurons. First, we determined the levels of *cyr61* mRNA at different developmental stages using RT-qPCR, both in our *in vitro* preparations and *in vivo*. As shown in Fig. 3*A*, the expression of *cyr61* mRNA was higher in still-developing hippocampal neurons (DIV7 and DIV10) than in mature hippocampal neurons (DIV14 and DIV17). *In vivo*, with the use of RNA isolated from the hippocampi of E18, P5, P10, P15, and P30 rats, we observed a significant decrease of *cyr61* expression between E18 and the postnatal period (Fig. 3*B*). However, differences observed during the postnatal period, although following a trend similar to cells maturing *in vitro*, did not reach statistical significance (Fig. 3*B*).

cyr61 is an immediate early gene, the expression of which is potentiated by several stimuli (see above). The results of our shRNA library screen prompted us to investigate whether BDNF and insulin, two factors important for dendritic arbor development (5, 33), induce higher *cyr61* mRNA levels in developing neurons. To achieve this, DIV8 neurons were first B27-starved overnight to equalize cellular responses and then treated with insulin (400 nM) or BDNF (100 ng/ml) for 1 h. As shown in Fig. 3, *C* and *D*, both insulin and BDNF increased *cyr61* mRNA levels. Pretreatment with actinomycin D (ActD), a transcription inhibitor, prevented these increases (Fig. 3, *C* and *D*), confirming that *cyr61* expression in our model undergoes transcriptional regulation. Interestingly, *cyr61* expression could still be induced, despite very low basal levels, in mature DIV21 neurons by insulin, BDNF, and 50 μM bicuculline, an antagonist of γ-aminobutyric acid A receptors that are responsible for inhibitory transmission (Fig. 3*E*).

Receptors for insulin and BDNF act via two major signaling pathways, PI3K and ERK. Consequently, we tested whether both pathways are needed for the insulin- and BDNF-induced transcription of *cyr61.* As shown in Fig. 3, *F* and *G*, pretreatment of neurons with wortmannin, an inhibitor of PI3K, prevented the increase in *cyr61* mRNA levels in both cases. Pretreatment of neurons with UO126, an inhibitor of MEK1/2, prevented the increase in *cyr61* mRNA levels in response to BDNF (Fig. 3*G*). Also, in the case of insulin stimulation, we observed a moderate inhibitory effect of UO126, which, however, did not reach statistical significance (Fig. 3*F*). There were no statistically significant differences between the following variants: ActD and ActD/insulin, ActD and ActD/BDNF,

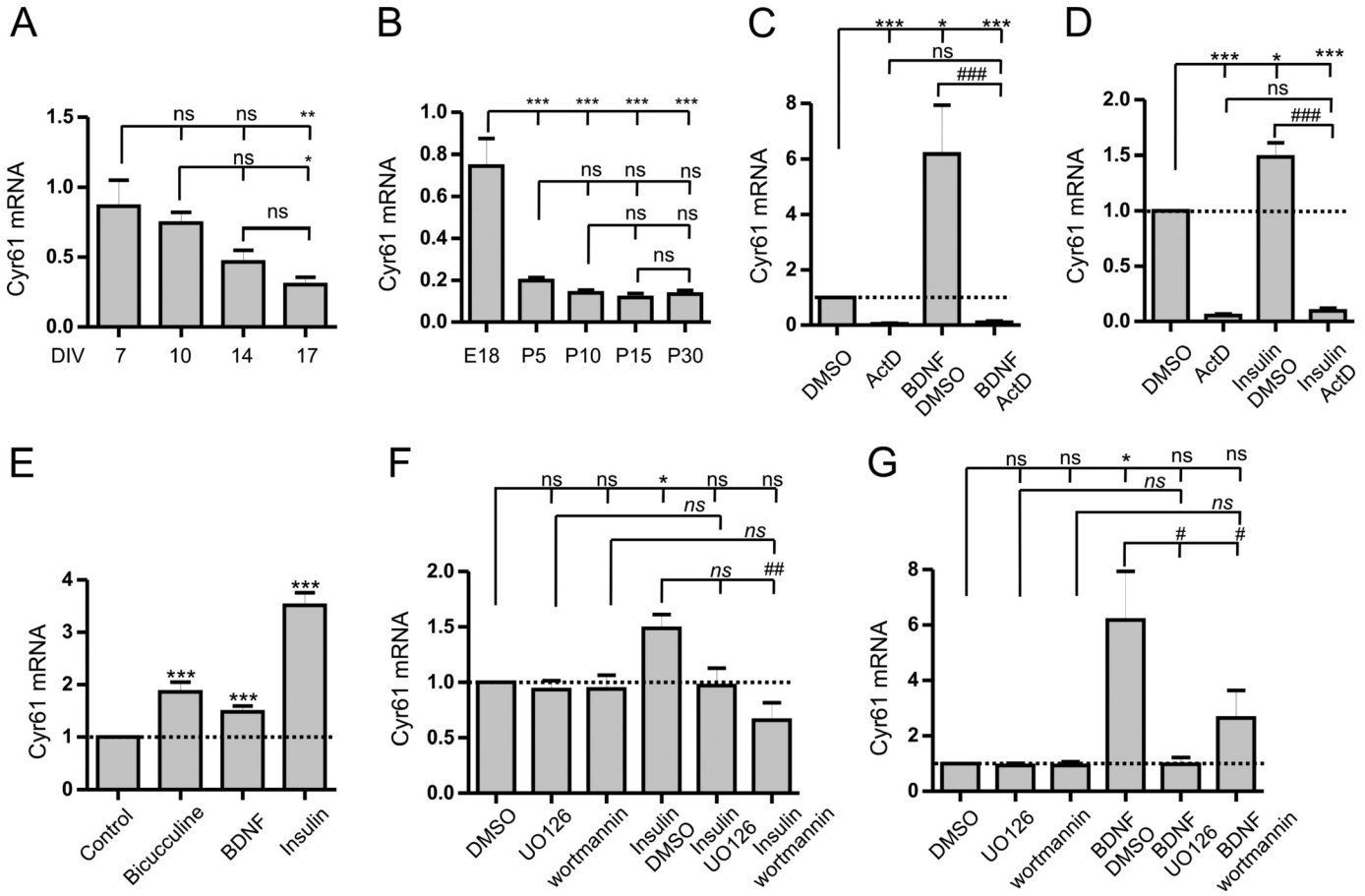

FIGURE 3. **Cyr61 is expressed in cultured hippocampal neurons and rat hippocampus and can be induced by insulin and BDNF treatment.** *cyr61* expression was assessed by RT-qPCR and quantified relative to GAPDH. *A*, *cyr61* expression in cultured hippocampal neurons on the indicated days *in vitro*. The plot represents the $2^{(-\Delta\Delta Ct)}$ mean values ± S.E. (*error bars*) (DIV7, $n = 4$; DIV10, $n = 4$; DIV14, $n = 3$; DIV17, $n = 4$). **, $p < 0.01$; *, $p < 0.05$; *ns*, not significant (one-way ANOVA test followed by Tukey's multiple comparison test). *B*, *cyr61* expression in rat hippocampi from animals on the indicated embryonic (*E*) or postnatal (*P*) days. The plot represents $2^{(-\Delta\Delta Ct)}$ mean values ± S.E. ($n = 3$ for each experimental group). ***, $p < 0.01$; *ns*, not significant (one-way ANOVA test followed by Tukey's multiple comparison test). *C*, *D*, *F*, and *G*, hippocampal neurons cultured *in vitro* (DIV8) were incubated overnight in medium with reduced B27 and stimulated with insulin or BDNF for 1 h. DMSO (control), actinomycin D, UO-126, or wortmannin was added to the medium 45 min prior to stimulation. Cyr61 expression in single experiments was compared with controls treated with DMSO. The plots represent mean values ± S.E. from six independent experiments. ***, $p < 0.001$; *, $p < 0.05$; *ns*, not significant compared with control value = 1 (one-sample *t* test). ###, $p < 0.001$; ##, $p < 0.01$; #, $p < 0.05$; *ns*, not significant compared as indicated (paired *t* test). *E*, hippocampal neurons cultured *in vitro* (DIV21) were incubated for 4 h in a medium without B27 and stimulated with bicuculline, insulin, or BDNF for 1 h. Cyr61 expression in single experiments was compared with untreated controls. The plot represents mean values ± S.E. from four independent experiments. ***, $p < 0.001$ compared with control value = 1 (one-sample *t* test).

UO126 and UO126/insulin, wortmannin and wortmannin/insulin, UO126 and UO126/BDNF, and wortmannin and wortmannin/BDNF. Both PI3K and MEK1/2 can stimulate mTOR activity. To provide evidence of the dependence of *cyr61* transcription on mTOR, we treated DIV8 neurons with 20 nM rapamycin for either 1 or 3 h. Because of the typical response of immediate early genes to protein synthesis inhibitors, *cyr61* mRNA levels dramatically increased (data not shown), precluding further pharmacological analysis of the direct effects of mTOR on *cyr61* transcription. Thus, we concluded that the expression of *cyr61* in response to BDNF stimulation depends on PI3K and ERK signaling, whereas insulin-dependent *cyr61* expression relies more strongly on PI3K in neurons.

Cyr61 Is Indispensable for Proper Dendritic Arbor Morphology of Developing but Not Mature Neurons under Basal Culture Conditions—Once we confirmed that *cyr61* is expressed in hippocampal neurons cultured *in vitro* at the time of intensive dendritogenesis and that it is regulated by factors that induce this process, we then returned to the analysis of the effects of Cyr61 on the dendritic arbors of hippocampal neurons. We first confirmed that our Cyr61 shRNAs down-regulated *cyr61* mRNA. To achieve this, we first nucleofected DIV0 cortical neurons with pSuper, pSuper-Cyr61sh#1, -sh#2, or -sh#3 or a pool of all three plasmids. However, the transfection of such young neurons with shRNAs against Cyr61 was lethal (data not shown). Therefore, we decided to use a non-neuronal rat cell line and nucleofected Cyr61 shRNAs to RAT2 cells. As shown in Fig. 4*A*, the pool of Cyr61 shRNAs as well as Cyr61sh#2 and -sh#3 effectively decreased the levels of endogenous *cyr61* mRNA measured with the use of RT-qPCR 48 h after nucleofection. Cyr61sh#1 also decreased Cyr61 mRNA, but this decrease did not reach statistical significance (but see Fig. 5).

For further verification of the specificity of a phenotypic effect caused by our Cyr61 shRNAs, we used a battery of standard approaches: (i) shRNA pool separation, (ii) scrambled shRNA overexpression, and (iii) phenotype "rescue" (45). Regarding the first approach, we transfected DIV8 neurons for 4 days with pSuper that encoded Cyr61sh#1, -sh#2, or -sh#3. As

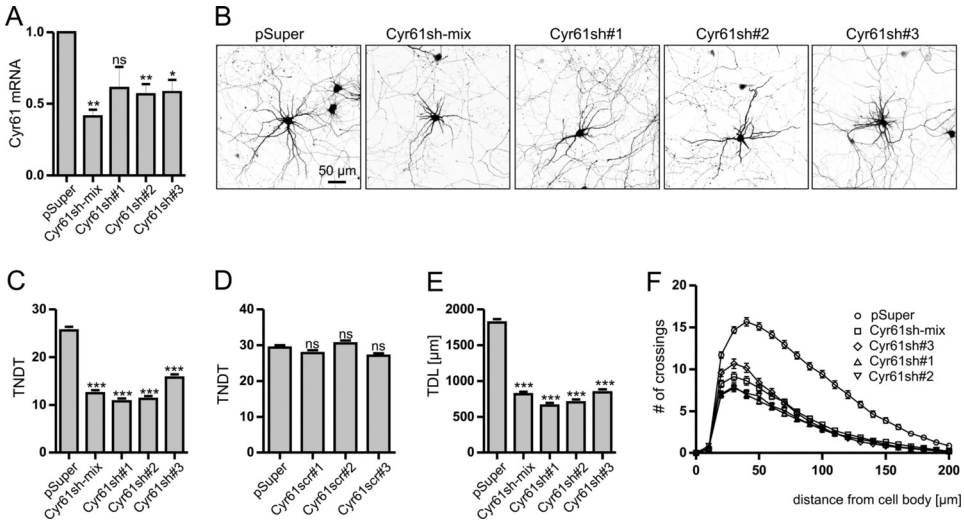

FIGURE 4. **Knockdown of Cyr61 in developing neurons simplifies dendritic tree morphology.** *A*, Cyr61shRNA validation was performed after nucleofection of RAT2 cells with pSuper, Cyr61sh#1, -sh#2, or -sh#3 or a pool of shRNAs. The cells were lysed 2 days after nucleofection, and Cyr61 mRNA levels were assessed by RT-qPCR, quantified relative to GAPDH, and compared with pSuper-nucleofected controls. The plot represents the mean values ± S.E. (*error bars*) from four independent experiments. **, $p < 0.01$; *, $p < 0.05$, compared with control value = 1 (one-sample *t* test); *ns*, not significant. *B*, representative images of cultured *in vitro* rat hippocampal neurons transfected on DIV8 for 4 days with pSuper vector (control) or plasmids that encode individual Cyr61sh or their pool (Cyr61sh-mix). The GFP-encoding plasmid was cotransfected for the visualization of transfected cells. *Scale bar*, 50 μm. *C*, TNDT of neurons transfected as described in *B*. Cell images were obtained from three independent culture batches. The data are expressed as mean values ± S.E. (pSuper, $n = 53$; Cyr61sh-mix, $n = 58$; Cyr61sh#1, $n = 51$; Cyr61sh#2, $n = 42$; Cyr61sh#3, $n = 47$). ***, $p < 0.001$, compared with pSuper (Kruskal-Wallis test followed by Dunn's post hoc test). *D*, TNDT of neurons transfected with either pSuper or scrambled shRNA vector and GFP-encoding plasmid as described in *B*. Cell images were obtained from three independent culture batches (pSuper, $n = 54$; Cyr61scr#1, $n = 55$; Cyr61scr#2, $n = 45$; Cyr61scr#3, $n = 51$). The data are expressed as mean values ± S.E. *ns*, not significant (compared with pSuper; Kruskal-Wallis test followed by Dunn's post hoc test). Shown are TDL (mean values ± S.E.) (*E*) and Sholl analysis (*F*) of neurons transfected as described in *B* (cell numbers as in *C*). ***, $p < 0.001$, compared with pSuper (Kruskal-Wallis test followed by Dunn's post hoc test; see supplemental Table 3 for detailed statistics for *F*).

a negative control, we used pSuper. As a positive control, we transfected cells with pooled Cyr61 shRNAs similarly to our initial screen (Fig. 2). Again, GFP-encoding plasmid was cotransfected for the identification of transfected cells and visualization of their morphology. As shown in Fig. 4, *B* and *C*, each of the tested Cyr61sh and their pool significantly decreased TNDT compared with pSuper-transfected cells. However, we did not observe any significant changes in TNDT when we repeated the experiments using their scrambled counterparts instead of Cyr61 shRNAs (Fig. 4*D*), which did not silence *cyr61* expression nucleofected to RAT2 cells (data not shown). Because effects of Cyr61 on dendrites were not previously reported, to additionally confirm that in case of Cyr61 knockdown our morphological criteria for dendrite selection are correct, we independently repeated experiment using either pSuper or Cyr61 shRNA pool transfection and quantified the number of MAP2-positive/Tau (PHF-1)-negative neurites. With such criteria we also showed that Cyr61 knockdown results in a significant decrease in the number of dendrites (pSuper/GFP ($n = 50$), 22.58 ± 0.72; Cyr61sh-mix ($n = 46$), 16.09 ± 0.61; $p < 0.001$; Mann-Whitney test). Because embryonic hippocampal cultures are mixtures of a large population of excitatory and a small population of inhibitory (glutamic acid decarboxylase (GAD67)-positive) neurons, we tested if knockdown of Cyr61 affects selectively one of them. Toward this end, we analyzed dendritic arbors of GAD67-positive cells transfected with either pSuper or Cyr61sh-mix and did not see any differences (data not shown). This suggests that Cyr61 knockdown selectively affects excitatory neurons.

The analysis of the additional parameters that describe dendritic arbor morphology also revealed the requirement of Cyr61 for proper dendritic arbor morphology. The TDL was decreased by 64, 61, and 54% for Cyr61sh#1, -sh#2, and -sh#3, respectively (Fig. 4*E*). These effects of individual Cyr61 shRNAs on TDL were comparable with the one obtained by the pool of shRNAs (55% reduction in TDL). We also used Sholl analysis of the dendritic fields of neurons that lack Cyr61 and confirmed their shrinkage. Specifically, the Sholl plots were strongly shifted downward and slightly leftward (Fig. 4*F* and supplemental Table 3). The number of maximum crosses was significantly lower (8.0 ± 0.4, 7.8 ± 0.4, 10.7 ± 0.6, and 9.1 ± 0.5 for the Cyr61sh#1, -sh#2, -sh#3, and Cyr61sh pool, respectively, compared with 15.7 ± 0.5 for pSuper) and reached closer to the cell soma in Cyr61 shRNA-transfected cells (pSuper, 40 μm; Cyr61sh#1, -sh#2, -sh#3, and the Cyr61sh pool, 30 μm; Fig. 4*E*).

To unequivocally confirm the specificity of the observed effects of Cyr61 knockdown on dendritic arbor morphology, we "rescued" the Cyr61 knockdown phenotype overexpressing GFP-tagged Cyr61. We took advantage of the fact that Cyr61sh#3 targets the 3′-untranslated region (UTR) of endogenous rat Cyr61 mRNA, which is spared in the plasmid that encodes Cyr61-GFP (Fig. 5*A*). Indeed, as shown in Fig. 5*B*, when we transfected DIV8 neurons for 4 days with Cyr61-GFP and either pSuper or pSuper-Cyr61sh#3, we did not observe substantial differences in the levels of GFP fluorescence. However, when we used pSuper-Cyr61sh#1 or -sh#2 for cotransfection with Cyr61-GFP, GFP fluorescence was greatly diminished (Fig. 5*B*). In all four cases, the fluorescence of mRFP, the cDNA of which was cotransfected for the visualization of transfected cells, remained intact (Fig. 5*B*). We next tested whether the transfection of Cyr61-GFP reverses the deleterious effects of a Cyr61 knockdown on neuronal dendritic arbors. Indeed, over-

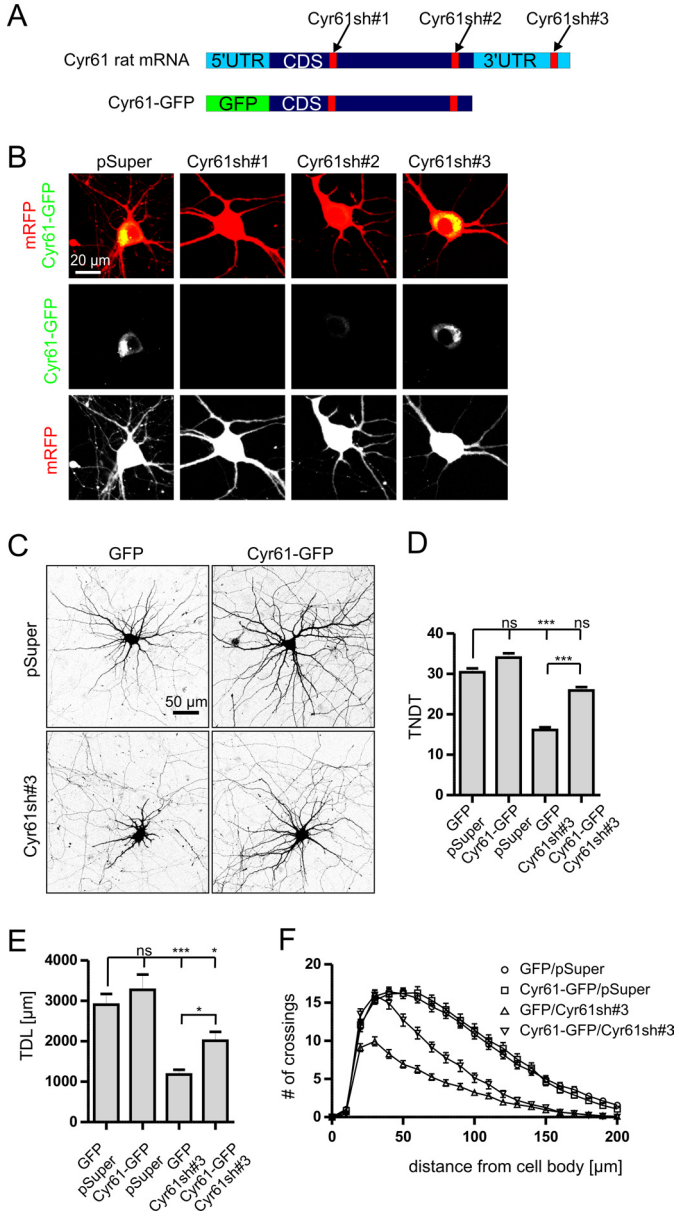

FIGURE 5. **Effect of Cyr61sh on TNDT is specific and can be rescued by overexpressing Cyr61-GFP.** *A*, schematic representation of Cyr61 mRNA and Cyr61-GFP coding sequence and localization of sequences targeted by Cyr61shRNAs. Note that Cyr61sh#1 and Cyr61sh#2 target both mRNA and the Cyr61-GFP coding sequence, whereas Cyr61sh#3 recognizes the sequence in the 3′-UTR of mRNA, absent in Cyr61-GFP. *B*, representative images of hippocampal neurons transfected on DIV8 with β-actin-Cyr61-GFP together with Cyr61sh#1, -sh#2, or -sh#3 or an empty pSuper vector and fixed after 4 days. mRFP-encoding plasmid was cotransfected to visualize transfected cells. *Scale bar*, 20 μm. *C*, representative images of rat hippocampal neurons cultured *in vitro* transfected on DIV8 for 4 days with either pSuper or pSuper-Cyr61sh#3 together with β-actin-GFP or β-actin-Cyr61-GFP. mRFP-encoding plasmid was cotransfected to visualize the morphology of transfected cells. *Scale bar*, 50 μm. Shown are TNDT (*D*), TDL (*D*), and Sholl analysis (*F*) of neurons transfected as in *C*. Cell images were obtained from three independent culture batches (pSuper/GFP, $n = 38$; pSuper/Cyr61-GFP, $n = 37$; Cyr61sh#3/GFP, $n = 41$; Cyr61sh#3/Cyr61-GFP, $n = 37$). The data are expressed as mean values ± S.E. (*error bars*). ***, $p < 0.001$; *, $p < 0.05$; *ns*, not significant (Kruskal-Wallis test followed by Dunn's post hoc test for *D* and *E*; see supplemental Table 3 for detailed statistics for *F*).

expression of Cyr61-GFP fully reversed the negative effects of Cyr61sh#3 on TNDT (Fig. 5, *C* and *D*). As expected, 4-day overexpression of Cyr61sh#3 without the rescue construct decreased TNDT (Fig. 5, *C* and *D*). The overexpression of Cyr61-GFP alone for the same time had no significant effect on dendritic arbors (Fig. 5, *C* and *D*). Also, using analysis of TDL and Sholl analysis, we confirmed the ability of Cyr61-GFP to rescue the effects of Cyr61 knockdown (Fig. 5, *E* and *F*, and supplemental Table 3). However, similar to our previous observations, rescue of more complex parameters of a dendritic arbor was only partial (33, 36, 37). Based on the above results, we concluded that the effects of Cyr61 knockdown on dendritic arbor morphology are specific. Because the pool of shRNAs acted similarly to separate shRNAs, we decided to use only pooled shRNAs that allow the use of lower doses of individual shRNAs, thereby reducing potential off-target effects.

The experiments described thus far suggested that the expression of *cyr61* is relatively high in developing neurons and needed for proper dendritic arborization at this stage. The expression of *cyr61* significantly dropped at the time of neuronal maturation and dendritic arbor stabilization. Therefore, we tested whether the morphology of the dendritic trees of mature neurons that express low levels of Cyr61 still rely on this protein. To achieve this, DIV15 neurons were transfected with the Cyr61 shRNA pool for 4 days (Fig. 6*A*). Neurons transfected with pSuper were used as a control. Similar to the previous experiments, GFP was cotransfected for neuronal morphology visualization. In contrast to developing neurons, Cyr61 knockdown in mature cells did not cause any differences in TNDT or TDL compared with the control (Fig. 6, *A*–*C*). The Sholl analysis did not reveal any major differences in the dendritic fields of these cells (Fig. 6*D* and supplemental Table 3). Thus, we concluded that Cyr61 is needed for the proper dendritic arbor morphology of developing but not mature neurons under basal culture conditions.

Cyr61 Knockdown Prevents Insulin-, Ras-ERK-, and Ras-PI3K-driven Dendritic Arborization—We identified Cyr61 in a screen of mTOR-dependent proteins required for dendritic arborization and found that *cyr61* expression is controlled by insulin and the PI3K and ERK pathways. mTOR activity was previously shown to be needed for the induction of dendritic growth of developing neurons both by insulin (33) and overexpression of constitutively active Ras mutants that specifically activate ERKs (RasV12S35) and PI3K (RasV12C40) (5). Therefore, we tested whether Cyr61 is needed for dendritic arborization in three independent models of mTOR-dependent growth established previously in our laboratory, namely chronic insulin treatment under B27-reduced cultured conditions (33), overexpression of constitutively active Ras mutants (5), and overproduction of constitutively active PI3K (5, 36). We first used our pharmacological model of dendritic arbor growth (33). To determine whether Cyr61 is essential for insulin-induced growth, we compared the dendritic arbors of neurons transfected on DIV8 with pSuper or a pool of shRNAs that target Cyr61, starved of B27, and chronically treated with insulin. A GFP-encoding vector was used to visualize the morphology of transfected cells. As shown in Fig. 7, *A*–*C*, the transfection of the Cyr61 shRNA pool resulted in lower TNDT and TDL in response to insulin compared with pSuper-transfected controls. In fact, these measures were identical when compared with non-stimulated neurons transfected with the Cyr61

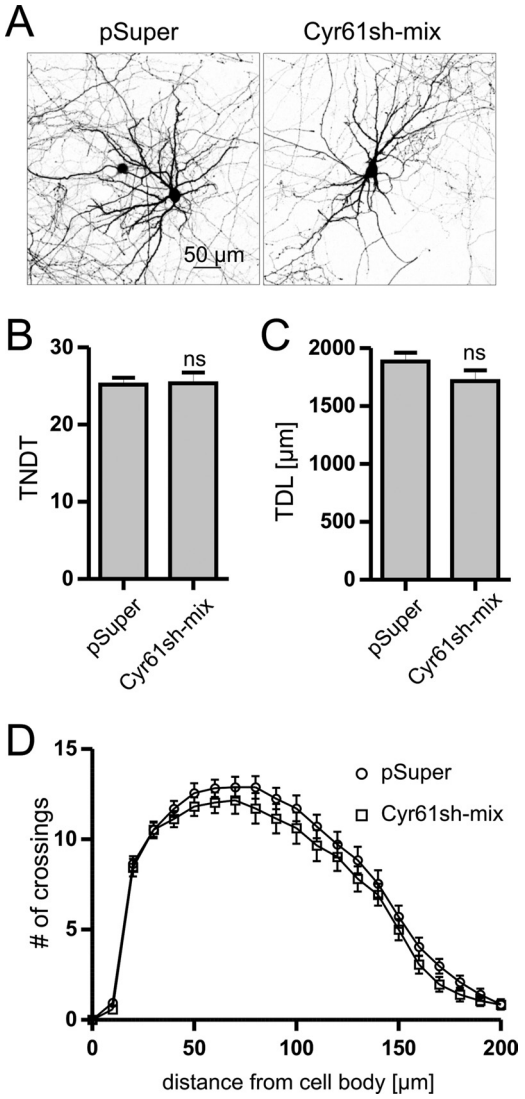

FIGURE 6. **Cyr61 knockdown in mature neurons does not disrupt dendritic tree morphology.** *A*, representative images of rat hippocampal neurons cultured *in vitro* and transfected on DIV15 for 4 days with pSuper vector (control) or a pool of plasmids that encode Cyr61sh#1, -sh#2, and -sh#3 (Cyr61sh-mix). GFP-encoding plasmid was cotransfected for the visualization of transfected cells. *Scale bar*, 50 μm. Shown are TNDT (*B*), TDL (*C*), and Sholl analysis (*D*) of neurons transfected as in *A*. Cell images were obtained from three independent culture batches (pSuper, $n = 36$; Cyr61sh-mix, $n = 32$). The data are expressed as mean values ± S.E. (*error bars*). *ns*, not significant (Mann-Whitney test for *B* and *C*; two-way ANOVA test followed by Bonferroni's post hoc test in *D*).

shRNA pool. Similar results were obtained with Sholl analysis (Fig. 7*D* and supplemental Table 3).

We then determined the importance of Cyr61 for dendritic growth in our two genetic models of induced dendritogenesis. In the first case, we transfected DIV8 neurons with the constitutively active Ras mutants RasV12, RasV12S35, and RasV12C40 for 5 days and observed a substantial increase in TNDT in all three cases compared with control cells transfected with EFα-β-gal (Fig. 8, *A* and *B*). When any of the Ras mutants were expressed together with the Cyr61sh pool, Ras-induced growth was completely blocked and not significantly different from cells transfected with β-gal and Cyr61 shRNA pool (Fig. 8, *A* and *B*). On the other hand, overexpression of Cyr61scr pool did not prevent Ras-induced dendritic arborization (Fig. 8*C*).

To obtain more detailed insight into changes of dendritic arbor caused by Ras overexpression combined with Cyr61 knockdown, we performed TDL and Sholl analyses. As shown in Fig. 8*D*, overexpression of Ras mutants potently increased TDL, and this effect was blocked by knockdown of Cyr61. As shown previously (5), overexpression of Ras mutants caused upward and rightward shifts of Sholl plot, and these effects were blocked by cotransfection of Cyr61 shRNA pool (Fig. 8*E* and supplemental Table 3). Altogether, our data suggest that Cyr61 is indeed needed for Ras-induced dendritic growth that relies on either ERK or PI3K. To further corroborate this conclusion, we tested whether constitutively active Ras and its more specific variants are capable of increasing *cyr61* expression. To achieve this, we nucleofected freshly isolated cortical neurons (37) with a constitutively active mutant of Ras (RasV12) and its variants that selectively activate either the PI3K (RasV12C40) or ERK (RasV12S35) pathway (5). All three mutants were effectively expressed in neurons upon nucleofection and increased the amount of *cyr61* mRNA compared with control neurons transfected with EFα-β-gal (Fig. 8, *F* and *G*). It should be noted, however, that the Ras mutant expression levels were not equal (Fig. 8*F*).

We previously showed that RasV12S35 and RasV12C40 control neuronal development in an mTOR-dependent fashion (5). Therefore, in a last series of experiments, we focused on PI3K-induced dendritic arborization, which is well documented to depend on mTOR (5, 40). DIV8 neurons were transfected with p110CAAX or EFα-β-gal (*i.e.* a negative control) together with pSuper or the pool of Cyr61sh for 5 days (Fig. 9*A*). We observed a substantial increase in TNDT and TDL of p110CAAX-transfected cells compared with control cells transfected with EFα-β-gal (Fig. 9, *A* and *B*). Also, the Sholl plot was shifted upward and rightward (Fig. 9*C* and supplemental Table 3). However, when p110CAAX was expressed together with the Cyr61sh pool, PI3K-induced growth was blocked (Fig. 9, *A*–*C*). On the other hand, when we used the Cyr61 scrRNA pool, the PI3K-induced growth was sustained (data not shown). Using nucleofection, we showed that RasV12C40, which should selectively induce only the PI3K pathway, increases *cyr61* mRNA levels in young neurons. We could not use this approach, however, for p110CAAX because of the poor expression of p110CAAX after nucleofection with the Amaxa system (data not shown). Thus, to prove that p110CAAX overexpression in neurons can increase *cyr61* mRNA levels, we transfected DIV8 hippocampal cells in culture with Lipofectamine2000 and performed FISH to detect *cyr61* transcripts. As shown in Fig. 9*E*, our antisense Cyr61 probe gave a higher signal than the sense one. However, p110CAAX overexpression for 2 days was able to further increase *cyr61* mRNA levels in transfected cells compared with EFα-β-gal-transfected control neurons or surrounding non-transfected cells (Fig. 9, *F* and *G*). Therefore, we concluded that Cyr61 is indispensable for the acquisition of proper dendritic morphology in models of mTOR-dependent dendritic growth when dendritic development is enhanced by insulin, Ras-ERK, or Ras-PI3K and that its mRNA level depends on these signaling pathways.

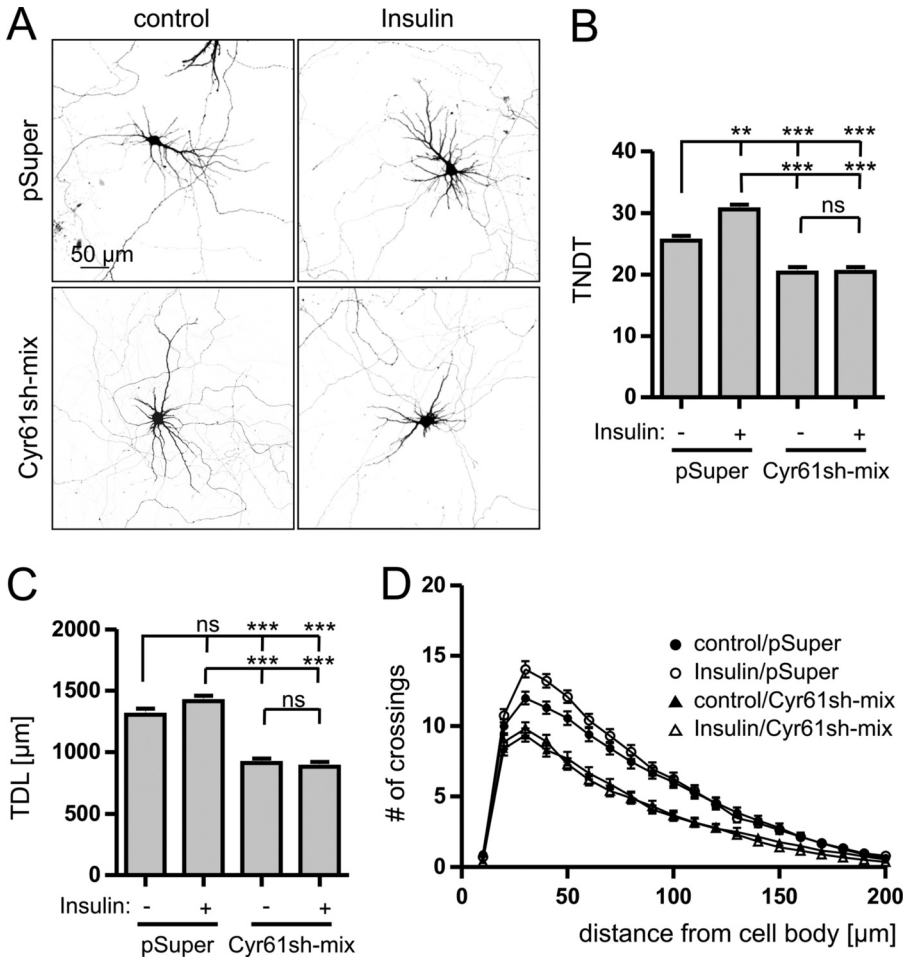

FIGURE 7. **Cyr61 knockdown inhibits dendritic growth induced by insulin.** *A*, representative images of hippocampal neurons cultured *in vitro*; transfected on DIV8 with pSuper or a pool of Cyr61sh#1, -sh#2, and -sh#3 (Cyr61sh-mix); and cultured under conditions of reduced B27 concentration. GFP was cotransfected for the visualization of transfected neurons. To induce dendritogenesis, insulin was added 4 h after transfection and then every 24 h until cell fixation on DIV12. *Scale bar*, 50 μm. Shown are TNDT (*B*), TDL (*C*), and Sholl analysis (*D*) of neurons transfected and treated as described in *A*. Cell images were obtained from three independent culture batches (control/pSuper, $n = 60$; insulin/pSuper, $n = 60$; control/Cyr61sh-mix, $n = 59$; insulin/Cyr61sh-mix, $n = 60$). The data are expressed as mean values ± S.E. (*error bars*). ***, $p < 0.001$; **, $p < 0.01$; *ns*, not significant (Kruskal-Wallis test followed by Dunn's post hoc test for *B* and *C*; see supplemental Table 3 for detailed statistics for *D*).

Cyr61 Is Sufficient to Induce Dendritic Growth of both Developing and Mature Neurons—Our experiments revealed that Cyr61 is required for the proper dendritic arbor morphology of developing neurons and suggested that 4-day overexpression of Cyr61-GFP was not sufficient for the induction of dendritic growth in such neurons (Fig. 5). However, evidence was provided previously that relatively short, 3-day overproduction of constitutively active PI3K was also not sufficient to induce the expansion of dendritic arbors (5). Thus, we tested whether longer 6-day overproduction of Cyr61-GFP is able to increase dendritic arborization. First, we transfected DIV8 neurons with either β-actin-GFP (negative control) or β-actin-Cyr61-GFP (Fig. 10*A*). β-Actin-mRFP was added to transfection mixtures to help visualize the morphology of transfected neurons. Six-day Cyr61-GFP overexpression increased TNDT by 42% compared with GFP-overproducing cells (Fig. 10*B*). The TDL also increased by 26% (Fig. 10*C*). Finally, the Sholl plot was significantly shifted upward, starting from 20 μm until 140 μm from the cell soma (Fig. 10*D* and supplemental Table 3). Consequently, the number of crossings in a maximum branching point increased from 16.7 ± 0.6 to 21.6 ± 0.7 (Fig. 10*D*). Additionally, the maximum branching point was shifted rightward in Cyr61-GFP-overexpressing cells (50 and 70 μm for GFP and Cyr61-GFP overexpression, respectively; Fig. 10*D*). Similar to experiments described above for Cyr61 knockdown, we independently confirmed that Cyr61 overexpression affects dendrites, counting the number of MAP2-positive/Tau (PHF-1)-negative neurites of control and Cyr61-overexpressing neurons. Using this approach, we showed that Cyr61 overexpression results in a significant increase of dendrite number (GFP/TdTomato ($n = 53$), 18.98 ± 0.68; Cyr61-GFP/TdTomato ($n = 40$), 22.23 ± 0.63; $p < 0.01$; Mann-Whitney test). We also tested if Cyr61 overexpression affects GAD67-positive cells and did not see any differences when compared with control (data not shown).

Although Cyr61 appeared spare for morphology of dendritic arbors of mature neurons, we asked whether increasing Cyr61 levels in such neurons could modify already established dendritic morphology. Neurons on DIV15 were transfected similarly to DIV8 neurons and fixed 6 days later. As shown in Fig. 10, *E–H*, and supplemental Table 3, overproduction of Cyr61-GFP in mature cells effectively increased the number of dendritic

tips and TDL and induced the expansion of dendritic fields compared with GFP-expressing controls. Altogether, these data demonstrated that Cyr61 overexpression is capable of inducing dendritic field expansion in both developing and mature neurons.

Cyr61 Controls Dendritic Arbor Morphology via β1-Integrin—How Cyr61 regulates dendritic morphology at the molecular level is currently unknown. Cyr61 is a ligand of β1-integrin (CD29) in fibroblasts (46, 47). β1-Integrin is also crucial for proper dendritic arbor morphology (48, 49). If Cyr61 acts via β1-integrin, then the effects of Cyr61-GFP overexpression should be diminished by a β1-integrin-blocking antibody. Such a strategy was efficiently used recently for studying the role of matrix metalloproteinase-9 in the dynamics of dendritic spines

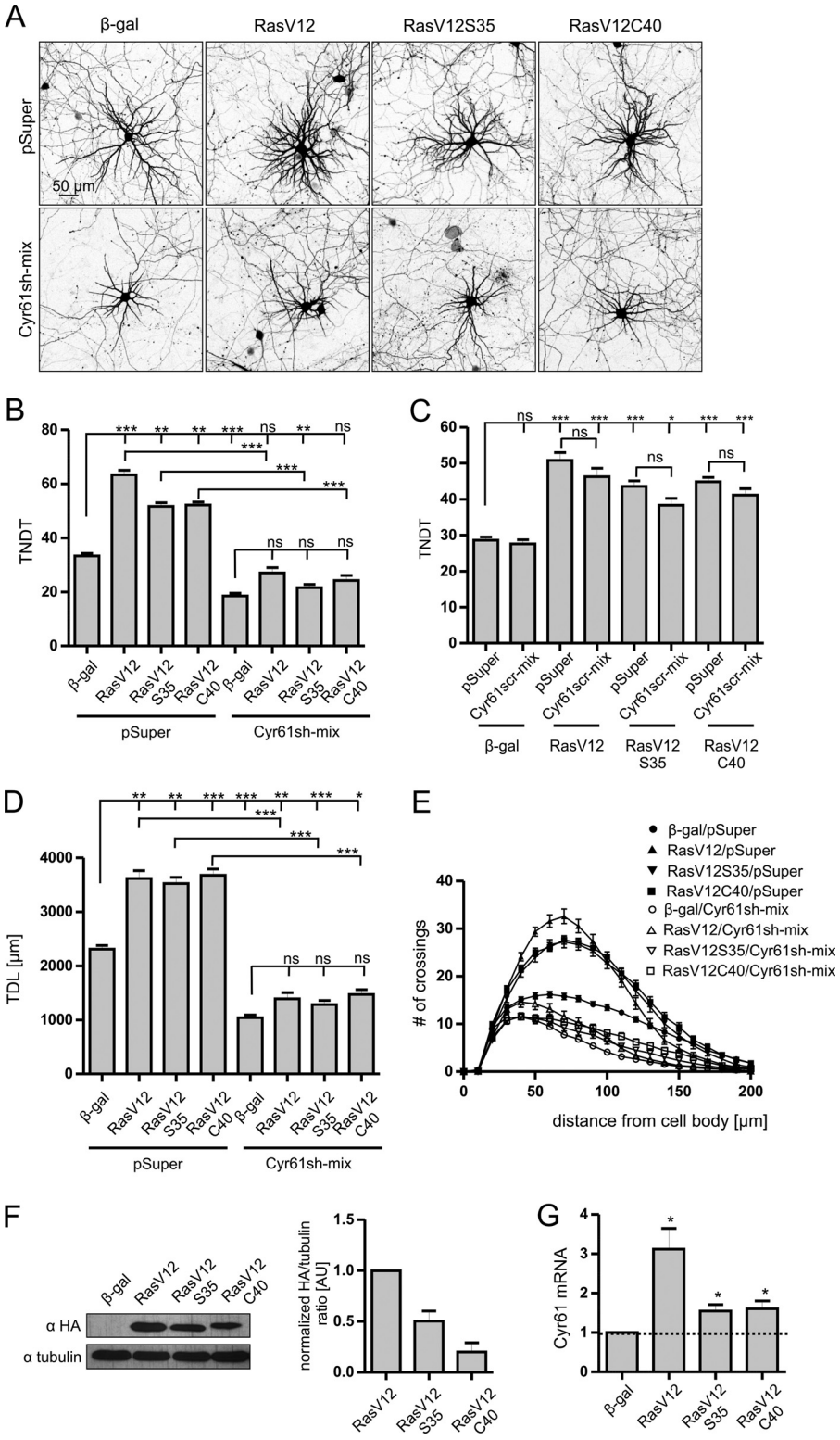

of hippocampal neurons (50). To test this hypothesis, DIV8 neurons were transfected with either a GFP- or Cyr61-GFP-encoding vector together with an mRFP-encoding vector to visualize neuronal morphology for 6 days. Two days post-transfection, the cells were treated with anti-CD29 antibody (20 μg/ml). The antibody was again added 4 days after transfection. As a control, the cells were exposed to the same concentration of isotypic antibody. Six-day overexpression of Cyr61-GFP in the presence of IgM increased TNDT compared with IgM-treated, GFP-overexpressing cells (Fig. 10, *I* and *J*). However, the application of an anti-CD29 antibody counterbalanced the effect of Cyr61 overexpression (Fig 10, *I* and *J*). Application of the anti-CD29 antibody did not have any significant effects on control cells transfected with β-actin-GFP (Fig. 10, *I* and *J*). This observation strongly implies that Cyr61 indeed regulates dendritic arborization via β1-integrin.

DISCUSSION

The present study showed that S6K1 is not sufficient for the control of dendritic growth as opposed to axonal development. This observation prompted us to perform shRNA screening for modifiers of the dendritic arbor, the transcription of which may depend on the mTOR pathway. As a result, the function of the matricellular protein Cyr61 in developing neurons was described for the first time. We showed that (i) *cyr61* was expressed in neurons during the time of intensive developmental dendritic arbor rearrangements; (ii) *cyr61* expression was increased by BDNF, insulin, Ras, and PI3K, known upstream activators of mTOR; and (iii) mTOR-dependent dendritic arborization induced by insulin, Ras, and PI3K was blocked by Cyr61 knockdown. Finally, we showed that Cyr61 overexpression induces the dendritic arborization of both developing and mature neurons, and this effect depended on β1-integrin.

We consider the observation that *cyr61* is expressed abundantly at the time of intensive dendritogenesis and is needed for this process to be the most important finding of the present work. We also showed that blocking β1-integrin prevented the positive effects of Cyr61 overexpression on dendritic arborization. The importance of Cyr61 for dendritic arbor development and the proposed mechanism that involves β1-integrin are further supported by previously published results that showed that (i) different integrins, including β1-integrin, serve as Cyr61 receptors (18, 20, 46) and (ii) β1-intergrin is important for dendritic arborization. Scholmann *et al.* (48) showed that β1-integrin is needed for semaphorin 3A-induced dendritic arborization in cultures *in vitro*. Recently, Warren *et al.* (49) confirmed the importance of this protein for the postnatal dendritic arbor development of hippocampal neurons *in vivo*. Interestingly, other CCN family members and angiogenic factors different from Cyr61 contribute to neuronal development. For example, CCN5 induces neurite outgrowth in a neuroblastoma Neuro2a cell line in an integrin-dependent manner (51). Licht *et al.* (52) showed that the angiogenic factor VEGF is necessary for the dendritic arbor development of adult-born interneurons that integrate into olfactory bulb circuitry. Another angiogenic protein, angiopoietin-1, was able to induce neurite outgrowth in PC12 cells (53) and increase the dendritic length of CA1 neurons when overexpressed *in vivo* (54).

An unanswered question is which signaling events contribute to dendritic growth downstream of Cyr61. Cyr61 was shown to activate small GTPase Rac1 in prostate cancer cells (55), which is a widely accepted activator of dendritic growth (3, 56, 57). Cyr61 can also act upstream of PI3K-mTOR and ERK signaling pathways (58, 59), raising the intriguing possibility that the initial activation of *cyr61* expression downstream of these kinases is an early step in a positive feedback loop that potentiates their progrowth effects and coordinates the actions of these kinases with remodeling of the extracellular matrix.

We previously showed that the canonical mTOR downstream target S6K1, which is involved in the control of translation, is needed for dendritic growth similarly to axonal growth (5, 6). However, the present study suggests that S6K1 activity is not sufficient to induce dendritic growth, as opposed to axonal growth. This prompted us to search for novel candidates that may be important for dendritic growth. We focused on proteins, the expression of which is potentially regulated by mTOR at the level of either transcription or mRNA stability. We chose this particular group for two reasons. First, these processes are crucial for dendritic growth (3, 4). Second, several groups reported the involvement of mTOR or its homologs in transcriptional control (8, 10, 60, 61). Our results (Fig. 2) showed that indeed several tested shRNA pools caused improper dendritic arborization. Among our positive hits, we focused on Cyr61 in this study, the physiological function of which has not been previously reported in neurons. We found that *cyr61* expression was increased by several upstream regulators of mTOR, such as insulin, BDNF, Ras, PI3K, and ERKs. However,

FIGURE 8. **Cyr61 knockdown inhibits dendritic growth induced by constitutively active Ras mutants.** *A*, representative images of hippocampal neurons transfected on DIV8 for 4 days as indicated. GFP-encoding plasmid was cotransfected for the visualization of transfected neurons. *Scale bar*, 50 μm. *B*, TNDT of transfected cells. Cell images were obtained from three independent culture batches (pSuper/β-gal, $n = 41$; pSuper/RasV12, $n = 40$; pSuper/RasV12S35, $n = 37$; pSuper/RasV12C40, $n = 40$; Cyr61sh-mix/β-gal, $n = 41$; Cyr61sh-mix/RasV12, $n = 37$; Cyr61sh-mix/RasV12S35, $n = 39$; Cyr61sh-mix/RasV12C40, $n = 36$). The data are expressed as mean values ± S.E. (*error bars*). ***, $p < 0.001$; **, $p < 0.01$; *ns*, not significant (Kruskal-Wallis test followed by Dunn's post hoc test). *C*, TNDT of hippocampal neurons transfected on DIV8 for 4 days as indicated. Cell images were obtained from three independent culture batches (pSuper/β-gal, $n = 39$; Cyr61scr-mix/β-gal, $n = 38$; pSuper/RasV12, $n = 38$; Cyr61scr-mix/RasV12, $n = 37$; pSuper/RasV12S35, $n = 37$; Cyr61scr-mix/RasV12S35, $n = 33$; pSuper/RasV12C40, $n = 38$; Cyr61scr-mix/RasV12C40, $n = 39$). The data are expressed as mean values ± S.E. ***, $p < 0.001$; *, $p < 0.05$; *ns*, not significant (Kruskal-Wallis test followed by Dunn's post hoc test). Shown are TDL (*D*) and Sholl analysis (*E*) of neurons transfected as described in *A* (cell numbers as in *C*). The data are expressed as mean values ± S.E. ***, $p < 0.001$; **, $p < 0.01$; *, $p < 0.05$; *ns*, not significant (Kruskal-Wallis test followed by Dunn's post hoc test for *D*; see supplemental Table 3 for detailed statistics for *E*). *F* and *G*, HA-tagged Ras active mutants (RasV12, RasV12S35, and RasV12C40) were expressed for 2 days in nucleofected cortical neurons. Nucleofection with β-gal-encoding plasmid was used as a control. *F*, representative results (*left*) and quantitative analysis of Western blot analysis of HA-tagged Ras mutant expression levels in nucleofected cortical neurons. Tubulin is shown as a loading control (*left*). The plot (*right*) represents the mean values ± S.E. of a ratio of HA signal to tubulin signal from five experiments. The HA/tubulin ratio for the RasV12 variant was treated as 1. *G*, results of RT-qPCR analysis of Cyr61 mRNA levels in cortical neurons nucleofected with either β-gal (control) or Ras mutant-encoding vectors. Cyr61 mRNA levels were quantified relative to GAPDH and compared with controls in each experiment. The plot represents the mean values ± S.E. from five independent experiments. ***, $p < 0.001$; **, $p < 0.01$; *, $p < 0.05$, compared with control value = 1 (one-sample *t* test); *ns*, not significant.

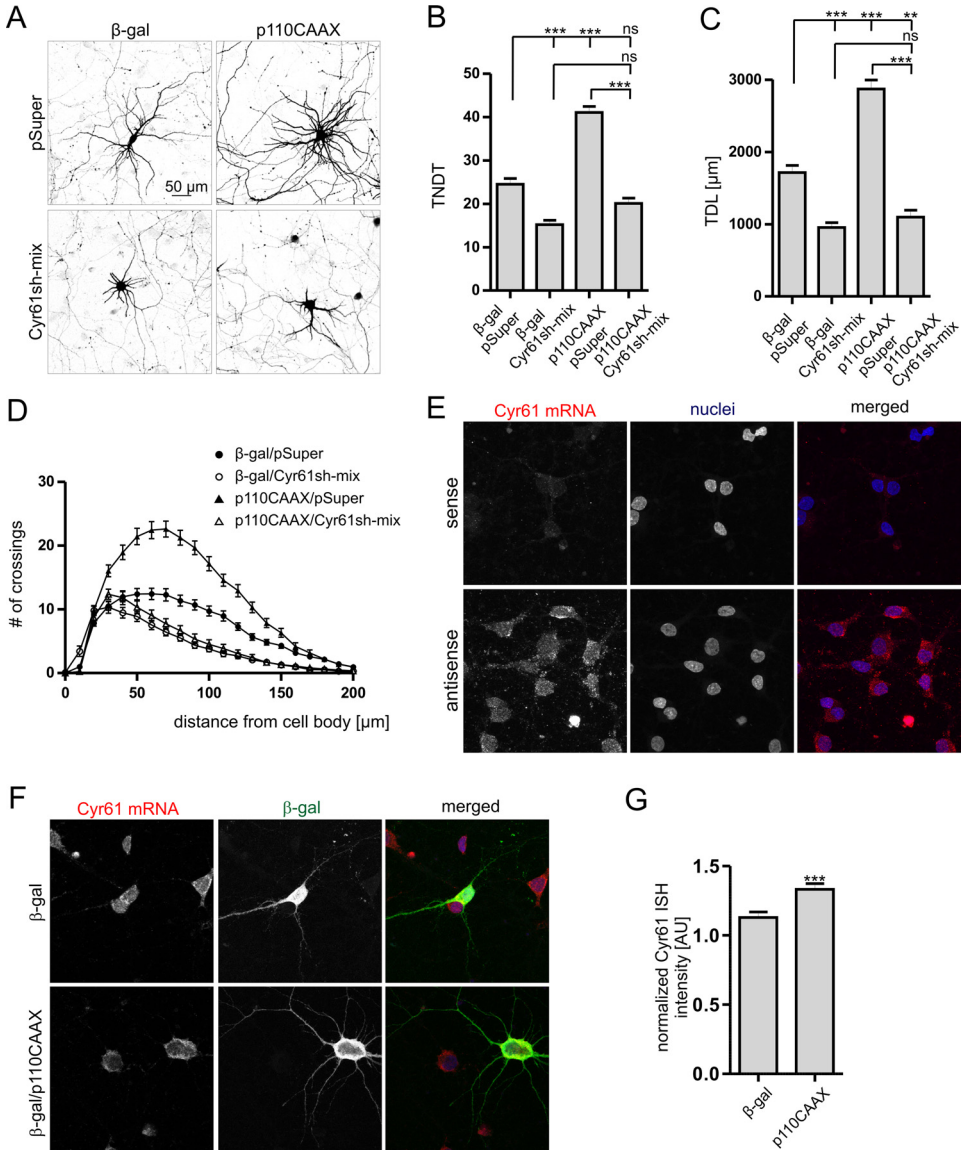

FIGURE 9. **Cyr61 knockdown inhibits dendritic growth induced by active PI3K.** *A*, representative images of hippocampal neurons transfected on DIV8 for 4 days as indicated. GFP-encoding plasmid was cotransfected for the visualization of transfected neurons. *Scale bar*, 50 μm. Shown are TNDT (*B*), TDL (*C*), and Sholl analysis (*D*) of transfected cells. Cell images were obtained from three independent culture batches (pSuper/β-gal, $n = 35$; Cyr61sh-mix/β-gal, $n = 35$; pSuper/p110CAAX, $n = 36$; Cyr61sh-mix/p110CAAX, $n = 35$). ***, $p < 0.001$, compared with pSuper/β-gal (Kruskal-Wallis test followed by Dunn's post hoc test; see supplemental Table 3 for detailed statistics for *D*). *E*, representative images of DIV10 hippocampal neurons stained by FISH with sense and antisense riboprobes against Cyr61 mRNA (*red*) and counterstained with Hoechst 33285 to visualize cell nuclei (*blue*). *F*, representative images of hippocampal neurons transfected on DIV8 for 2 days with either β-gal-encoding plasmid alone or plasmids that encode β-gal and p110CAAX, stained by FISH with antisense riboprobe against Cyr61 mRNA (*red*), and counterstained with β-gal antibody to identify transfected cells (*green*) and Hoechst 33285 to visualize cell nuclei (*blue*). *G*, quantification of mean intensity of FISH signal of cells transfected as in *F* standardized to mean intensity of FISH signal of neighboring non-transfected cells from the same image. Cell images were obtained from three independent culture batches (β-gal, $n = 31$; β-gal/p110CAAX, $n = 38$). The data are expressed as mean values ± S.E. (*error bars*). ***, $p < 0.001$, compared with β-gal (Mann-Whitney test).

we failed to directly prove the necessity of mTOR for *cyr61* transcription. This is because *cyr61* mRNA levels increased upon rapamycin treatment. This observation is consistent with the behavior of other immediate early genes, the transcripts of which are stabilized under conditions of protein translation inhibition. Thus, the potential involvement of mTOR in the control of *cyr61* transcription is currently only suggested by the indirect evidence discussed above. Additional support for this hypothesis comes from published studies. For example, *cyr61* expression is increased in mouse neuroepithelial cells that lack TSC2 (tuberous sclerosis complex 2) and are characterized by increased mTOR activity (17). However, we cannot exclude the possibility that the increased expression of some genes in such a model is mTOR-independent because this was not rigorously tested by the authors. Another line of reasoning derives from known mTOR links to some *cyr61* transcription regulators. The transcription factors involved in the control of *cyr61* expression in various cellular models include TCF4 (26), SRF (62), CBP (62), CREB (63), FOXO3a (64), AP1 (27, 63), STAT3 (65), and HIF1α (27). The most obvious link is HIF1α, known as an mTOR effector induced under hypoxic conditions (9). However, HIF1α can be activated in an oxygen-independent manner in neurons (15). We did not observe any significant effects of overexpression of either the dominant negative or constitu-

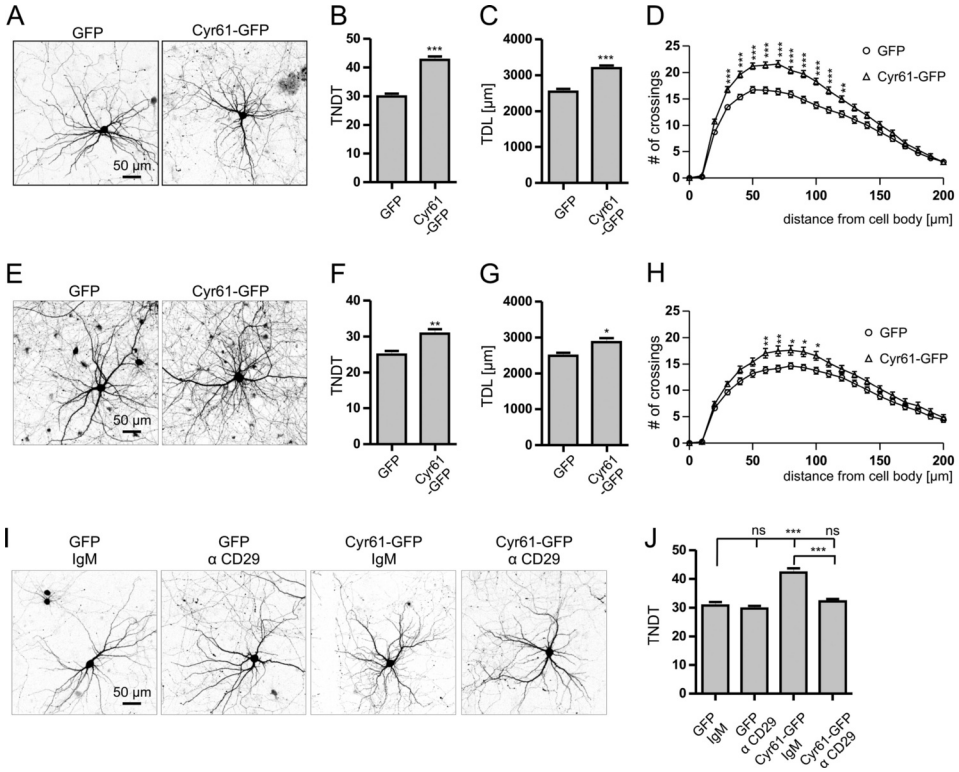

FIGURE 10. **Cyr61 overexpression induces dendritic tree growth in a β1-integrin-dependent manner.** *A*, representative images of hippocampal neurons transfected on DIV8 for 6 days with GFP or Cyr61-GFP-encoding plasmids. mRFP-encoding plasmid was cotransfected for the visualization of transfected cells. *Scale bar*, 50 μm. Shown are TNDT (*B*), TDL (*C*), and Sholl analysis (*D*) of neurons transfected as in *A*. Cell images were obtained from three independent culture batches (GFP, $n = 47$; Cyr61-GFP, $n = 40$). *E*, representative images of hippocampal neurons transfected on DIV15 for 6 days with GFP- or Cyr61-GFP-encoding plasmids. mRFP-encoding plasmid was cotransfected for the visualization of transfected cells. *Scale bar*, 50 μm. Shown are TNDT (*F*), TDL (*G*), and Sholl analysis (*H*) of neurons transfected as in *E*. Cell images were obtained from three independent culture batches (GFP, $n = 36$; Cyr61-GFP, $n = 38$). The data are expressed as mean values ± S.E. (*error bars*). ***, $p < 0.001$; **, $p < 0.01$; *, $p < 0.05$, Mann-Whitney test for *B*, *C*, *F*, and *G* or two-way ANOVA followed by Bonferroni's post hoc test for *D* and *H*. *I*, representative images of hippocampal neurons transfected on DIV8 for 6 days with GFP- or Cyr61-GFP-encoding plasmids. mRFP-encoding plasmid was cotransfected for the visualization of transfected cells. Anti-CD29 or control IgM antibody was added to the medium 2 and 4 days after transfection. *Scale bar*, 50 μm. *J*, TNDT of transfected cells. Cell images were obtained from three independent culture batches (GFP/IgM, $n = 42$; GFP/α-CD29, $n = 45$; Cyr61-GFP/IgM, $n = 46$; Cyr61-GFP/α-CD29, $n = 45$). The data are expressed as mean ± S.E. ***, $p < 0.001$ (Kruskal-Wallis test followed by Dunn's post hoc test); *ns*, not significant.

tively active mutants of this protein on the morphology of dendritic trees of hippocampal neurons (data not shown). STAT3 and STAT3-dependent transcription were shown to be regulated by the mTOR pathway in neuroblastoma cells treated with ciliary neurotrophic factor (66). The activity of two other transcription factors that regulate *cyr61* expression, CREB and FOXO, can be regulated by Akt. mTORC2 was shown to activate Akt (67) and is important for dendritic arborization in experimental models identical to those used in the present work (33). Thus, one could speculate that mTOR is engaged in the control of *cyr61* expression through the mTORC2 complex. However, *cyr61* expression is up-regulated in cells that lack TSC2 (17), which most likely decreases mTORC2 and Akt activity (68). Thus, the positive regulation of Cyr61 expression via the mTORC2-Akt pathway appears to be rather unlikely.

Importantly, transcription factors such as SRF (69), CBP, CREB (70), and AP1 (42) are also involved in the regulation of dendritic growth of different types of neurons, similar to mTOR and Cyr61. Thus, an intriguing question is whether these transcription factors can link dendritic growth stimulation with mTOR activation and the induction of *cyr61* transcription. Notably, however, all of these transcription factors in neurons can be regulated by the PI3K and ERK pathways, independent of mTOR. Therefore, this kinase might not be necessary for the activation of *cyr61* expression by these two signaling pathways. Thus, although the role of Cyr61 in shaping dendritic arbors is unequivocal, further studies are needed to directly prove the participation of mTOR in the control of *cyr61* expression during dendritogenesis and reveal the responsible transcription factors.

Acknowledgments—We thank Dr. Casper C. Hoogenraad for the β-actin-mRFP plasmid, Dr. Roger Y. Tsien for TdTomato cDNA, and Dr. Peter Davies and Dr. Jakub Wlodarczyk for sharing the PHF-1, CD-29, and IgM antibodies. We thank Drs. Lester Lau and Chih-Chiun Chen for useful technical comments. We thank Malgorzata Zarebska, Iwona Cymerman, Anna Urbanska, Katarzyna Debowska, Marta Wisniewska, Monika Dudek, Alina Zielinska, and Marcelina Pieprzyk for help with the experiments, statistical analysis, and organization.

REFERENCES

1. Stuart, G., Spruston, N., and Häusser, M. (2007) *Dendrites*, 2nd Ed., Oxford University Press, Oxford
2. Segev, I., and London, M. (2000) Untangling dendrites with quantitative models. *Science* **290,** 744–750

3. Urbanska, M., Blazejczyk, M., and Jaworski, J. (2008) Molecular basis of dendritic arborization. *Acta Neurobiol. Exp.* **68,** 264–288
4. Jan, Y. N., and Jan, L. Y. (2010) Branching out. Mechanisms of dendritic arborization. *Nat. Rev. Neurosci.* **11,** 316–328
5. Jaworski, J., Spangler, S., Seeburg, D. P., Hoogenraad, C. C., and Sheng, M. (2005) Control of dendritic arborization by the phosphoinositide-3′-kinase-Akt-mammalian target of rapamycin pathway. *J. Neurosci.* **25,** 11300–11312
6. Morita, T., and Sobue, K. (2009) Specification of neuronal polarity regulated by local translation of CRMP2 and Tau via the mTOR-p70S6K pathway. *J. Biol. Chem.* **284,** 27734–27745
7. Loewith, R. (2010) TORC1 in *The Enzymes* (Hall, M. N., and Tamanoi, F., eds) Vol. 27, pp. 147–175, Elsevier, Amsterdam
8. Guertin, D. A., Guntur, K. V., Bell, G. W., Thoreen, C. C., and Sabatini, D. M. (2006) Functional genomics identifies TOR-regulated genes that control growth and division. *Curr. Biol.* **16,** 958–970
9. Land, S. C., and Tee, A. R. (2007) Hypoxia-inducible factor 1α is regulated by the mammalian target of rapamycin (mTOR) via an mTOR signaling motif. *J. Biol. Chem.* **282,** 20534–20543
10. Cunningham, J. T., Rodgers, J. T., Arlow, D. H., Vazquez, F., Mootha, V. K., and Puigserver, P. (2007) mTOR controls mitochondrial oxidative function through a YY1-PGC-1α transcriptional complex. *Nature* **450,** 736–740
11. Peterson, T. R., Sengupta, S. S., Harris, T. E., Carmack, A. E., Kang, S. A., Balderas, E., Guertin, D. A., Madden, K. L., Carpenter, A. E., Finck, B. N., and Sabatini, D. M. (2011) mTOR complex 1 regulates lipin 1 localization to control the SREBP pathway. *Cell* **146,** 408–420
12. Shor, B., Wu, J., Shakey, Q., Toral-Barza, L., Shi, C., Follettie, M., and Yu, K. (2010) Requirement of the mTOR kinase for the regulation of Maf1 phosphorylation and control of RNA polymerase III-dependent transcription in cancer cells. *J. Biol. Chem.* **285,** 15380–15392
13. Rylski, M., Amborska, R., Zybura, K., Mioduszewska, B., Michaluk, P., Jaworski, J., and Kaczmarek, L. (2008) Yin Yang 1 is a critical repressor of matrix metalloproteinase-9 expression in brain neurons. *J. Biol. Chem.* **283,** 35140–35153
14. Taghibiglou, C., Martin, H. G., Lai, T. W., Cho, T., Prasad, S., Kojic, L., Lu, J., Liu, Y., Lo, E., Zhang, S., Wu, J. Z., Li, Y. P., Wen, Y. H., Imm, J. H., Cynader, M. S., and Wang, Y. T. (2009) Role of NMDA receptor-dependent activation of SREBP1 in excitotoxic and ischemic neuronal injuries. *Nat. Med.* **15,** 1399–1406
15. Huang, Y. F., Yang, C. H., Huang, C. C., Tai, M. H., and Hsu, K. S. (2010) Pharmacological and genetic accumulation of hypoxia-inducible factor-1α enhances excitatory synaptic transmission in hippocampal neurons through the production of vascular endothelial growth factor. *J. Neurosci.* **30,** 6080–6093
16. Tyburczy, M. E., Kotulska, K., Pokarowski, P., Mieczkowski, J., Kucharska, J., Grajkowska, W., Roszkowski, M., Jozwiak, S., and Kaminska, B. (2010) Novel proteins regulated by mTOR in subependymal giant cell astrocytomas of patients with tuberous sclerosis complex and new therapeutic implications. *Am. J. Pathol.* **176,** 1878–1890
17. Onda, H., Crino, P. B., Zhang, H., Murphey, R. D., Rastelli, L., Gould Rothberg, B. E., and Kwiatkowski, D. J. (2002) Tsc2 null murine neuroepithelial cells are a model for human tuber giant cells, and show activation of an mTOR pathway. *Mol. Cell Neurosci.* **21,** 561–574
18. Grzeszkiewicz, T. M., Kirschling, D. J., Chen, N., and Lau, L. F. (2001) CYR61 stimulates human skin fibroblast migration through Integrin $\alpha v\beta 5$ and enhances mitogenesis through integrin $\alpha v\beta 3$, independent of its carboxyl-terminal domain. *J. Biol. Chem.* **276,** 21943–21950
19. Leu, S. J., Chen, N., Chen, C. C., Todorovic, V., Bai, T., Juric, V., Liu, Y., Yan, G., Lam, S. C., and Lau, L. F. (2004) Targeted mutagenesis of the angiogenic protein CCN1 (CYR61). Selective inactivation of integrin $\alpha 6\beta 1$-heparan sulfate proteoglycan coreceptor-mediated cellular functions. *J. Biol. Chem.* **279,** 44177–44187
20. Chen, N., Leu, S. J., Todorovic, V., Lam, S. C., and Lau, L. F. (2004) Identification of a novel integrin $\alpha v\beta 3$ binding site in CCN1 (CYR61) critical for pro-angiogenic activities in vascular endothelial cells. *J. Biol. Chem.* **279,** 44166–44176
21. Lau, L. F. (2011) CCN1/CYR61. The very model of a modern matricellular protein. *Cell Mol. Life Sci.* **68,** 3149–3163
22. Chen, C. C., and Lau, L. F. (2009) Functions and mechanisms of action of CCN matricellular proteins. *Int. J. Biochem. Cell Biol.* **41,** 771–783
23. Latinkic, B. V., Mo, F. E., Greenspan, J. A., Copeland, N. G., Gilbert, D. J., Jenkins, N. A., Ross, S. R., and Lau, L. F. (2001) Promoter function of the angiogenic inducer Cyr61 gene in transgenic mice. Tissue specificity, inducibility during wound healing, and role of the serum response element. *Endocrinology* **142,** 2549–2557
24. Kim, K. H., Min, Y. K., Baik, J. H., Lau, L. F., Chaqour, B., and Chung, K. C. (2003) Expression of angiogenic factor Cyr61 during neuronal cell death via the activation of c-Jun N-terminal kinase and serum response factor. *J. Biol. Chem.* **278,** 13847–13854
25. Sampath, D., Winneker, R. C., and Zhang, Z. (2002) The angiogenic factor Cyr61 is induced by the progestin R5020 and is necessary for mammary adenocarcinoma cell growth. *Endocrine* **18,** 147–159
26. Li, Z. Q., Ding, W., Sun, S. J., Li, J., Pan, J., Zhao, C., Wu, W. R., and Si, W. K. (2012) Cyr61/CCN1 is regulated by Wnt/β-catenin signaling and plays an important role in the progression of hepatocellular carcinoma. *PLoS One* **7,** e35754
27. Kunz, M., Moeller, S., Koczan, D., Lorenz, P., Wenger, R. H., Glocker, M. O., Thiesen, H. J., Gross, G., and Ibrahim, S. M. (2003) Mechanisms of hypoxic gene regulation of angiogenesis factor Cyr61 in melanoma cells. *J. Biol. Chem.* **278,** 45651–45660
28. Tamura, I., Rosenbloom, J., Macarak, E., and Chaqour, B. (2001) Regulation of Cyr61 gene expression by mechanical stretch through multiple signaling pathways. *Am. J. Physiol. Cell Physiol.* **281,** C1524–C1532
29. Jicha, G. A., Lane, E., Vincent, I., Otvos, L., Jr., Hoffmann, R., and Davies, P. (1997) A conformation- and phosphorylation-dependent antibody recognizing the paired helical filaments of Alzheimer's disease. *J. Neurochem.* **69,** 2087–2095
30. Brummelkamp, T. R., Bernards, R., and Agami, R. (2002) A system for stable expression of short interfering RNAs in mammalian cells. *Science* **296,** 550–553
31. Hoogenraad, C. C., Feliu-Mojer, M. I., Spangler, S. A., Milstein, A. D., Dunah, A. W., Hung, A. Y., and Sheng, M. (2007) Liprin α1 degradation by calcium/calmodulin-dependent protein kinase II regulates LAR receptor tyrosine phosphatase distribution and dendrite development. *Dev. Cell* **12,** 587–602
32. Konopka, W., Duniec, K., Mioduszewska, B., Proszynski, T., Jaworski, J., and Kaczmarek, L. (2005) hCMV and Tet promoters for inducible gene expression in rat neurons *in vitro* and *in vivo*. *Neurobiol. Dis.* **19,** 283–292
33. Urbanska, M., Gozdz, A., Swiech, L. J., and Jaworski, J. (2012) Mammalian target of rapamycin complex 1 (MTORC1) and 2 MTORC2) control the dendritic arbor morphology of hippocampal neurons. *J. Biol. Chem.* **287,** 30240–30256
34. Shaner, N. C., Campbell, R. E., Steinbach, P. A., Giepmans, B. N., Palmer, A. E., and Tsien, R. Y. (2004) Improved monomeric red, orange and yellow fluorescent proteins derived from *Discosoma* sp. red fluorescent protein. *Nat. Biotechnol.* **22,** 1567–1572
35. Kaech, S., Ludin, B., and Matus, A. (1996) Cytoskeletal plasticity in cells expressing neuronal microtubule-associated proteins. *Neuron* **17,** 1189–1199
36. Swiech, L., Blazejczyk, M., Urbanska, M., Pietruszka, P., Dortland, B. R., Malik, A. R., Wulf, P. S., Hoogenraad, C. C., and Jaworski, J. (2011) CLIP-170 and IQGAP1 cooperatively regulate dendrite morphology. *J. Neurosci.* **31,** 4555–4568
37. Perycz, M., Urbanska, A. S., Krawczyk, P. S., Parobczak, K., and Jaworski, J. (2011) Zipcode binding protein 1 regulates the development of dendritic arbors in hippocampal neurons. *J. Neurosci.* **31,** 5271–5285
38. Meijering, E., Jacob, M., Sarria, J. C., Steiner, P., Hirling, H., and Unser, M. (2004) Design and validation of a tool for neurite tracing and analysis in fluorescence microscopy images. *Cytometry A* **58,** 167–176
39. Kaech, S., and Banker, G. (2006) Culturing hippocampal neurons. *Nat. Protoc.* **1,** 2406–2415
40. Kumar, V., Zhang, M. X., Swank, M. W., Kunz, J., and Wu, G. Y. (2005) Regulation of dendritic morphogenesis by Ras-PI3K-Akt-mTOR and Ras-MAPK signaling pathways. *J. Neurosci.* **25,** 11288–11299
41. Sholl, D. A. (1953) Dendritic organization in the neurons of the visual and

motor cortices of the cat. *J. Anat.* **87,** 387–406
42. Zhang, J., Zhang, L., Jiao, H., Zhang, Q., Zhang, D., Lou, D., Katz, J. L., and Xu, M. (2006) c-Fos facilitates the acquisition and extinction of cocaine-induced persistent changes. *J. Neurosci.* **26,** 13287–13296
43. Hsu, P. P., Kang, S. A., Rameseder, J., Zhang, Y., Ottina, K. A., Lim, D., Peterson, T. R., Choi, Y., Gray, N. S., Yaffe, M. B., Marto, J. A., and Sabatini, D. M. (2011) The mTOR-regulated phosphoproteome reveals a mechanism of mTORC1-mediated inhibition of growth factor signaling. *Science* **332,** 1317–1322
44. Yu, Y., Yoon, S. O., Poulogiannis, G., Yang, Q., Ma, X. M., Villén, J., Kubica, N., Hoffman, G. R., Cantley, L. C., Gygi, S. P., and Blenis, J. (2011) Phosphoproteomic analysis identifies Grb10 as an mTORC1 substrate that negatively regulates insulin signaling. *Science* **332,** 1322–1326
45. Svoboda, P. (2007) Off-targeting and other non-specific effects of RNAi experiments in mammalian cells. *Curr. Opin. Mol. Ther.* **9,** 248–257
46. Chen, N., Chen, C. C., and Lau, L. F. (2000) Adhesion of human skin fibroblasts to Cyr61 is mediated through integrin $\alpha 6\beta 1$ and cell surface heparan sulfate proteoglycans. *J. Biol. Chem.* **275,** 24953–24961
47. Leu, S. J., Lam, S. C., and Lau, L. F. (2002) Pro-angiogenic activities of CYR61 (CCN1) mediated through integrins $\alpha v\beta 3$ and $\alpha 6\beta 1$ in human umbilical vein endothelial cells. *J. Biol. Chem.* **277,** 46248–46255
48. Schlomann, U., Schwamborn, J. C., Müller, M., Fässler, R., and Püschel, A. W. (2009) The stimulation of dendrite growth by Sema3A requires integrin engagement and focal adhesion kinase. *J. Cell Sci.* **122,** 2034–2042
49. Warren, M. S., Bradley, W. D., Gourley, S. L., Lin, Y. C., Simpson, M. A., Reichardt, L. F., Greer, C. A., Taylor, J. R., and Koleske, A. J. (2012) Integrin $\beta 1$ signals through Arg to regulate postnatal dendritic arborization, synapse density, and behavior. *J. Neurosci.* **32,** 2824–2834
50. Michaluk, P., Wawrzyniak, M., Alot, P., Szczot, M., Wyrembek, P., Mercik, K., Medvedev, N., Wilczek, E., De Roo, M., Zuschratter, W., Muller, D., Wilczynski, G. M., Mozrzymas, J. W., Stewart, M. G., Kaczmarek, L., and Wlodarczyk, J. (2011) Influence of matrix metalloproteinase MMP-9 on dendritic spine morphology. *J. Cell Sci.* **124,** 3369–3380
51. Ohkawa, Y., Ohmi, Y., Tajima, O., Yamauchi, Y., and Furukawa, K. (2011) Wisp2/CCN5 up-regulated in the central nervous system of GM3-only mice facilitates neurite formation in Neuro2a cells via integrin-Akt signaling. *Biochem. Biophys. Res. Commun.* **411,** 483–489
52. Licht, T., Eavri, R., Goshen, I., Shlomai, Y., Mizrahi, A., and Keshet, E. (2010) VEGF is required for dendritogenesis of newly born olfactory bulb interneurons. *Development* **137,** 261–271
53. Chen, X., Fu, W., Tung, C. E., and Ward, N. L. (2009) Angiopoietin-1 induces neurite outgrowth of PC12 cells in a Tie2-independent, $\beta 1$-integrin-dependent manner. *Neurosci. Res.* **64,** 348–354
54. Ward, N. L., Putoczki, T., Mearow, K., Ivanco, T. L., and Dumont, D. J. (2005) Vascular-specific growth factor angiopoietin 1 is involved in the organization of neuronal processes. *J. Comp. Neurol.* **482,** 244–256
55. Sun, Z. J., Wang, Y., Cai, Z., Chen, P. P., Tong, X. J., and Xie, D. (2008) Involvement of Cyr61 in growth, migration, and metastasis of prostate cancer cells. *Br. J. Cancer* **99,** 1656–1667
56. Hayashi, K., Ohshima, T., and Mikoshiba, K. (2002) Pak1 is involved in dendrite initiation as a downstream effector of Rac1 in cortical neurons. *Mol. Cell Neurosci.* **20,** 579–594
57. Nakayama, A. Y., Harms, M. B., and Luo, L. (2000) Small GTPases Rac and Rho in the maintenance of dendritic spines and branches in hippocampal pyramidal neurons. *J. Neurosci.* **20,** 5329–5338
58. Su, J. L., Chiou, J., Tang, C. H., Zhao, M., Tsai, C. H., Chen, P. S., Chang, Y. W., Chien, M. H., Peng, C. Y., Hsiao, M., Kuo, M. L., and Yen, M. L. (2010) CYR61 regulates BMP-2-dependent osteoblast differentiation through the $\alpha v\beta 3$ integrin/integrin-linked kinase/ERK pathway. *J. Biol. Chem.* **285,** 31325–31336
59. Zhang, X., Ding, L., Diao, Z., Yan, G., Sun, H., and Hu, Y. (2012) CYR61 modulates the vascular endothelial growth factor C expression of decidual NK cells via PI3K/AKT pathway. *Am. J. Reprod. Immunol.* **67,** 216–223
60. Tsang, C. K., Liu, H., and Zheng, X. F. (2010) mTOR binds to the promoters of RNA polymerase I- and III-transcribed genes. *Cell Cycle* **9,** 953–957
61. Huber, A., French, S. L., Tekotte, H., Yerlikaya, S., Stahl, M., Perepelkina, M. P., Tyers, M., Rougemont, J., Beyer, A. L., and Loewith, R. (2011) Sch9 regulates ribosome biogenesis via Stb3, Dot6 and Tod6 and the histone deacetylase complex RPD3L. *EMBO J.* **30,** 3052–3064
62. Hanna, M., Liu, H., Amir, J., Sun, Y., Morris, S. W., Siddiqui, M. A., Lau, L. F., and Chaqour, B. (2009) Mechanical regulation of the proangiogenic factor CCN1/CYR61 gene requires the combined activities of MRTF-A and CREB-binding protein histone acetyltransferase. *J. Biol. Chem.* **284,** 23125–23136
63. Han, J. S., Macarak, E., Rosenbloom, J., Chung, K. C., and Chaqour, B. (2003) Regulation of Cyr61/CCN1 gene expression through RhoA GTPase and p38MAPK signaling pathways. *Eur. J. Biochem.* **270,** 3408–3421
64. Lee, H. Y., Chung, J. W., Youn, S. W., Kim, J. Y., Park, K. W., Koo, B. K., Oh, B. H., Park, Y. B., Chaqour, B., Walsh, K., and Kim, H. S. (2007) Forkhead transcription factor FOXO3a is a negative regulator of angiogenic immediate early gene CYR61, leading to inhibition of vascular smooth muscle cell proliferation and neointimal hyperplasia. *Circ. Res.* **100,** 372–380
65. Bourillot, P. Y., Aksoy, I., Schreiber, V., Wianny, F., Schulz, H., Hummel, O., Hubner, N., and Savatier, P. (2009) Novel STAT3 target genes exert distinct roles in the inhibition of mesoderm and endoderm differentiation in cooperation with Nanog. *Stem Cells* **27,** 1760–1771
66. Yokogami, K., Wakisaka, S., Avruch, J., and Reeves, S. A. (2000) Serine phosphorylation and maximal activation of STAT3 during CNTF signaling is mediated by the rapamycin target mTOR. *Curr. Biol.* **10,** 47–50
67. Sarbassov, D. D., Guertin, D. A., Ali, S. M., and Sabatini, D. M. (2005) Phosphorylation and regulation of Akt/PKB by the rictor-mTOR complex. *Science* **307,** 1098–1101
68. Yang, Q., Inoki, K., Kim, E., and Guan, K. L. (2006) TSC1/TSC2 and Rheb have different effects on TORC1 and TORC2 activity. *Proc. Natl. Acad. Sci. U.S.A.* **103,** 6811–6816
69. Stritt, C., and Knöll, B. (2010) Serum response factor regulates hippocampal lamination and dendrite development and is connected with reelin signaling. *Mol. Cell Biol.* **30,** 1828–1837
70. Redmond, L., Kashani, A. H., and Ghosh, A. (2002) Calcium regulation of dendritic growth via CaM kinase IV and CREB-mediated transcription. *Neuron* **34,** 999–1010